NATIONAL ADVISORY COMMITTEE FOR AERONAUTICS

TECHNICAL NOTE 3213

TRANSONIC FLOW PAST CONE CYLINDERS

By George E. Solomon

California Institute of Technology

NACA

Washington

September 1954

NATIONAL ADVISORY COMMITTEE FOR AERONAUTICS

TECHNICAL NOTE 3213

TRANSONIC FLOW PAST CONE CYLINDERS

By George E. Solomon

SUMMARY

Experimental results are presented for transonic flow past cone-cylinder, axially symmetric bodies. The drag coefficient and surface Mach number are studied as the free-stream Mach number is varied and, wherever possible, the experimental results are compared with theoretical predictions. Interferometric results for several typical flow configurations are shown and an example of shock-free supersonic-to-subsonic compression is experimentally demonstrated.

The theoretical problem of transonic flow past finite cones is discussed briefly and an approximate solution of the axially symmetric transonic equations, valid for a semi-infinite cone, is presented.

INTRODUCTION

Transonic flow past certain two-dimensional bodies has been the subject of several recent papers and the phenomena are well understood. The theoretical results of Cole (ref. 1), Guderley and Yoshihara (ref. 2), Vincenti and Wagoner (ref. 3), and others apply to two-dimensional symmetrical double-wedge airfoils. The experimental results of Bryson (ref. 4) and Griffith (ref. 5) substantiate the theoretical work in a very satisfactory manner. More recently, Vincenti and Wagoner (ref. 6) and Guderley and Yoshihara (ref. 7) have analyzed the transonic flow past two-dimensional unsymmetrical sections, that is, lifting double-wedge airfoils. Current experiments on lifting double-wedge airfoils (ref. 8) at the Guggenheim Aeronautical Laboratory of the California Institute of Technology indicate that agreement between theoretical and experimental results will again be obtained.

Two-dimensional and axially symmetric transonic flows are of considerable theoretical and practical interest since these two specialized problems are limiting cases of the more complex problem of the flow about an arbitrary three-dimensional body.

The study of axially symmetric transonic flow is not so complete as that of two-dimensional flow. In recent years several papers, notably

those of Von Kármán (ref. 9) and Oswatitsch and Berndt (ref. 10), have
studied the similarity rules of axially symmetric transonic flow. Also,
Yoshihara (ref. 11) has calculated the flow about a finite cone at a
free-stream Mach number of 1 by a relaxation technique and has obtained
some experimental verification of the theoretical result. The hodograph
problem for general transonic flow past finite cones is discussed in
reference 8. However, theoretical solutions or experimental results for
the complete transonic regime are not, at present, available. The pres-
ent paper presents the results of an experimental investigation of the
transonic flow past cone-cylinder bodies. A conical tip followed by a
cylindrical afterbody was chosen as the experimental model for two pri-
mary reasons: (1) The relatively simple geometry of a cone-cylinder
body may simplify the theoretical problem, and (2) viscous effects are
minimized; that is, the boundary layer on the cone surface is in a
region of decreasing or constant pressure so that the presence of the
boundary layer will not greatly alter the shape of the body forward of
the cone shoulder.

Theoretical results for the supersonic flow past a cone were first
presented in 1929 by Busemann (ref. 12). Busemann's solution postulates
a semi-infinite cone and assumes that the flow is conical; that is,
along rays through the apex of the semi-infinite cone, the flow parame-
ters such as pressure and velocity are constant. The solution is found
by a geometrical construction in the hodograph plane and it is readily
apparent that a conical solution exists only so long as a shock wave is
attached to the cone apex and, therefore, the free-stream Mach number
is supersonic. It is interesting to note that Busemann's solution pre-
dicts smooth shock-free compression from supersonic to subsonic flow
for particular combinations of cone angle and free-stream Mach number.
The conical solution also shows that for a given cone angle and free-
stream Mach number M_∞ the surface Mach number is always less than the
Mach number immediately behind the conical shock wave; as M_∞ decreases,
the surface Mach number decreases and eventually passes from supersonic
to subsonic values. As was mentioned by Busemann, the conical solution
for a semi-infinite cone is completely valid for a finite cone so long
as the flow is everywhere supersonic, but when the surface Mach number
is less than sonic the perturbation due to the corner or shoulder of the
finite cone is propagated forward through the subsonic portion of the
field destroying the conicity of the flow. Thus, the Busemann solution
is completely valid for a finite cone only so long as M_∞ is large
enough so that the surface Mach number is greater than sonic.

Taylor and Maccoll (ref. 13) in 1933 presented the results of a
numerical integration of the axially symmetric equations of motion for
conical flow about semi-infinite cones and also presented experimental
verification of their theoretical results. Further experimental veri-
fication by Maccoll (ref. 14) was published in 1937. Both of the above
papers noted that deviations of the experiments from the theoretical

predictions, notably in the shape of the shock wave, are apparent when the surface Mach number is subsonic.

As was mentioned previously, Yoshihara (ref. 11) has computed, by relaxation methods, the flow about a cone cylinder at $M_\infty = 1.00$ and has experimentally verified the calculation. However, theoretical solutions do not exist for the complete transonic regime. Solutions have not been developed for the flow past a finite cone when M_∞ is subsonic or when M_∞ is between sonic and the value of M_∞ at which Busemann's conical solution becomes valid. Drougge (ref. 15) has computed the flow field between a detached shock wave and a finite cone by relaxation methods; however, the position and shape of the detached shock wave were determined initially from schlieren photographs.

The experimental results reported in this paper cover several interesting features of the transonic flow about finite cones. The deviations of the surface Mach number from the values predicted by conical theory are examined for values of M_∞ such that the flow field is transonic in nature. The behavior of the surface Mach number for subsonic values of M_∞, and as M_∞ approaches sonic from subsonic values, is examined in some detail so that an extrapolation to $M_\infty = 1.00$ may be made. The above surface Mach number data lead naturally to the evaluation of the drag coefficient, and experimental values of the drag coefficient in the transonic regime are presented.

The physical location of the sonic line in a meridional plane of the flow about a finite cone is of considerable interest for a theoretical study of the problem of axially symmetric flow. With this fact in mind, an interferometric analysis was made at several typical values of M_∞ so as to determine the local Mach number fields about finite cones. Several examples of supersonic to subsonic shock-free compression are experimentally demonstrated.

Experimental values of the shock-wave angle at the cone tip, particularly at values of M_∞ where the flow field between the shock wave and the cone surface is transonic or subsonic in nature, are presented, and a comparison with the values from conical theory is shown.

The conical solution for flow about a semi-infinite cone demonstrates that a conical solution does not exist if, for a given cone angle, M_∞ decreases below a certain minimum M_∞. This minimum M_∞ is defined to be the M_∞ for which shock-wave detachment occurs for a semi-infinite cone. Whether or not the shock-wave-detachment Mach number for a finite cone can be determined from conical theory is of considerable theoretical interest. Experimental values of the detachment distance of a shock wave from a finite cone tip, the distance obviously being zero at attachment, have been collected from several sources and the results analyzed in this report.

The transonic equations of motion and boundary conditions as derived by Von Kármán (ref. 9) for axially symmetric flow require several assumptions as to the relative magnitude of various terms in the exact equations of motion and the related boundary conditions. To demonstrate that the transonic equations retain the important features of the exact equations, an approximate solution of the problem of conical flow about a semi-infinite cone has been developed employing the transonic equations and boundary conditions. A comparison of the exact Busemann solution and the approximate transonic solution is presented in the report.

SYMBOLS

$$A_{ki} = \frac{\sqrt{(k+1)^2 - i^2} - \sqrt{k^2 - i^2}}{2k + 1}$$

a^* velocity of sound for $M_\infty = 1.00$

b width of increments of region of integration

C_D cone drag coefficient; reference area is cone base area

C_D^* drag coefficient at $M_\infty = 1.00$

C_p pressure coefficient, $\dfrac{2}{\gamma M_\infty^2} \left(\dfrac{p_s}{p_\infty} - 1\right)$

C_p^* pressure coefficient at $M_\infty = 1.00$

c chord of cone

d cone base diameter

i, k integers

l path length

M_s cone-surface Mach number

M_∞ free-stream Mach number

M_{sw} Mach number immediately downstream of a shock wave

N	number of outermost increment of region of integration
n	index of refraction of air
p_0	stagnation pressure
p_s	surface static pressure
p_∞	free-stream static pressure
$q_x,\ q_r$	velocities in axial and radial directions, respectively
r	radial distance from axis of symmetry to point on light path
r_b	cone base radius
S	interferometric fringe shift
u	nondimensional transonic axial-velocity perturbation in appendix C; y^2 in appendix B

$$u_s = y_s{}^2$$

v	nondimensional transonic radial-velocity perturbation in appendix C; r^2 in appendix B
v_0	v on surface of body

$$w = r^2$$

x	axial distance downstream of cone tip
y	perpendicular distance from axis of symmetry to light path
β	shock-wave angle
β_{w_n}	shock-wave angle at cone tip
γ	ratio of specific heats of air, 1.400
δ	axial distance from cone shoulder to shock wave

$$\zeta = M_\infty{}^2$$

$$\eta = r/x$$

η_s tangent of shock-wave angle

$\eta_1 = y/x$

θ cone semiangle

κ Gladstone-Dale constant

λ_0 wave length in vacuum of light employed

$\xi = M_s^2$

ρ density of air

$\rho(l)$ density of undetermined medium

ρ_R density of reference medium

ρ_∞ free-stream density

$\sigma = x/r$

ϕ perturbation potential

EXPERIMENTAL EQUIPMENT

Wind Tunnel

The transonic wind tunnel at GALCIT is a continuous-flow wind tunnel. For supersonic testing, the test-section Mach number may be continuously varied over a wide range by altering the shape of one flexible wall. The test-section Mach number is varied by changing the area of a sonic throat downstream of the test section when subsonic tests are being performed. The test-section width is 4 inches and the height is 9 inches. The design of the flexible test-section wall is discussed in reference 16.

Interferometer

The interferometer used in the present investigation is of the Mach-Zehnder type. Both light paths of the interferometer are passed through the wind-tunnel test section, one beam passing through the flow region under analysis and the other beam passing through the undisturbed flow in the test section upstream of the model. The fringe shifts due to density variations in the boundary layer are eliminated since both beams pass

through the boundary layer on the test-section walls and are affected almost equally. The growth of the boundary layer between the two beams is not compensated by the above arrangement, but the effect is of secondary importance. A detailed description of the GALCIT interferometer and a very complete bibliography on interferometer construction is given in reference 17.

Models

The models were conical-tipped brass cylinders of 20°, 25°, and 30° semiangle. The base diameters were between 0.30 and 0.50 inch. Thus, the Reynolds numbers for the tests, with the base diameter of the models as the reference dimension, varied from 55,000 to 143,000. The tips of the cones were made as sharp as possible and the maximum tip diameter of the dullest of the models was approximately 1/3 percent of its base diameter. Also, the models were black-nickel plated to improve the photographic definition. The angle of attack and angle of yaw were adjusted to zero by equalizing the pressure on the cone surface at four annular points.

EXPERIMENTAL TECHNIQUES

Interferometry

An experimental investigation of flow phenomena is facilitated by the employment of an interferometer to determine the density fields in gaseous (or liquid) flows. The interferometer technique possesses the obvious advantage of eliminating the need for placing any type of probe into a flow region where the presence of the probe may completely alter the undisturbed flow field. A disadvantage is also present, however, since the values of density are not immediately available as the test is in progress. A more serious disadvantage is the fact that the interferometer integrates the density values on its light paths (see appendix A) and, thus, the measurement of density is not localized but is influenced by inhomogeneities in the flow which may be well removed from the points of interest.

Two general types of flow are amenable to interferometric analysis, namely, two-dimensional and axially symmetric flow. This paper is concerned solely with axially symmetric flow analysis. A discussion of the method employed to reduce the finite-fringe interferograms, such as figure 1, to density distributions may be found in appendix A. The method is essentially that outlined in reference 18. An excellent discussion of axially symmetric data reduction is given in reference 19 where several references to earlier papers in the field will be found.

These earlier papers are mainly concerned with evaluating the interferometer-data reduction techniques for axially symmetric flow by investigating the flow about cone cylinders at Mach numbers and cone angles where the Busemann conical solution was known to be valid. Reference 20 presents some experimental results in the same general flow regimes as are investigated in this report.

Sonic-Line Location by Wave Reflection

The location of the sonic line in a meridional plane of an axially symmetric transonic flow can be determined experimentally by at least three distinct methods. The first method is by static-pressure measurements, the second is by interferometric analysis, and the third is that of Mach wave reflection from the sonic line. It should be noted that at the point of reflection the Mach wave will be perpendicular to the streamline direction through the sonic line.

To locate the sonic line within the flow about a cone, a small-diameter probe was placed in the free-stream flow outside of the cone shock wave. The probe was in a position such that the probe shock wave pierced the cone shock wave and entered the flow field about the cone. The shock waves formed by the probe closely approximate Mach waves at large distances from the probe and a typical wave reflection is shown in figure 2. The perturbations in the flow about the cone caused by the waves do not appreciably affect the position of the sonic line as shown by figure 3 where a comparison is made of the location of the sonic line as found by interferometric analysis and by the wave-reflection method. The probe method is much more convenient than the pressure-measurement or interferometric method since the phenomenon may be observed with a schlieren system, so that the result is obtained visually.

Pressure Measurements

The pressure measurements in this investigation were made either on a micromanometer (accuracy of ± 0.01 millimeter of mercury) or on a nomograph Mach meter (ref. 21).

EXPERIMENTAL RESULTS AND DISCUSSION

General Flow Characteristics

An analysis of the flow of a compressible fluid about an axially symmetric finite cone, that is, a cone cylinder, indicates that five distinct regimes of flow are possible. These regimes are given below.

Regime I.- Regime I is subsonic flow at infinity with a region of locally supersonic flow downstream of the cone shoulder. A schlieren photograph of this type of flow is shown in figure 4. It should be noted that an extremely weak shock wave originates at the cone shoulder and terminates at the downstream "normal" shock wave. The forked appearance of the base of the terminating "normal" shock wave is an illusion caused by the axial symmetry of the flow. The light rays which pass near the surface of the body in the region of the rearward branch of the "fork" also pass through the outer portion of the shock and the spurious rearward branch is caused by the light-ray deflections in the outer portion of the shock wave. A meridional section of the shock wave actually includes only the front branch of the fork.

Regime II.- Regime II is supersonic flow at infinity with a detached shock wave and subsonic flow between the shock wave and the cone. Figure 1 is a finite-fringe interferogram of this type of flow.

Regime III.- Regime III is supersonic flow at infinity with an attached curved shock wave and subsonic flow between the initial portion of the shock wave and the cone. A schlieren photograph of this flow is shown in figure 5(a). Taylor and Maccoll's original paper on conical flow (ref. 13) includes a schlieren photograph of an attached curved shock.

Regime IV.- Regime IV is supersonic flow at infinity with an attached shock wave and mixed supersonic and subsonic flow between the shock wave and the cone. A schlieren photograph of this flow is shown in figure 5(b).

Regime V.- Regime V is supersonic flow at infinity with completely supersonic flow between the attached shock wave and the cone surface. The Busemann solution applies in this regime and has been verified experimentally in references 13, 14, 19, and 22.

Local Mach Number Contours

The local Mach number contours in a meridional plane for the flow about a 25° semiangle cone are shown in figure 6 for flow regimes II, III, and IV. The local Mach number contours for a 30° semiangle cone in regime II are shown in figure 7. These data were obtained by interferometric analysis as discussed in appendix A.

The local Mach number contours should be normal to the cone surface since the cone surface is a flat boundary and any pressure gradient at the surface must be parallel to the flat surface. However, near the shoulder of the cone cylinder the surface is curved by the effect of the corner expansion on the boundary layer, and thus the local Mach number

contours are not quite perpendicular to the cone surface immediately
ahead of the shoulder.

Sonic-Line Location

The location of the sonic line can be determined by interferometric
analysis, but a more useful method, in the present investigation, was the
wave-reflection method. The location of the sonic line in regimes II,
III, and IV is discussed below.

Regime II.- Examples of the sonic-line location in regime II are
shown in figures 6(a) and 6(b). The sonic line originates at the cone
shoulder and terminates on the detached shock wave. In figure 7 it may
be seen that a region of supersonic to subsonic compression exists on the
outer portion of the sonic line. The sonic line actually originates
slightly upstream of the cone shoulder. This effect is due to the
rounding of the cone shoulder by the surface boundary layer.

Regime III.- Figure 6(c) illustrates the case of the flow with a
nearly attached curved shock wave. Again, a small region of supersonic
to subsonic compression is present on the outer portion of the sonic
line. The free-stream Mach number is slightly less than the detach-
ment M_∞ predicted by the exact conical theory. The question of experi-
mental detachment Mach number is discussed below.

Regime IV.- Several examples of the sonic-line location in regime IV
are shown in figures 3, 6(d), and 8. Figure 3 shows the location as
determined by interferometric means and as determined by wave reflection.
The sonic line again originates at the corner and now terminates at the
cone tip and not on the shock wave as in regimes II and III. A shock-
free supersonic-to-subsonic compression occurs on the forward portion of
the sonic line. The location of the sonic line for a 20° semiangle cone
is shown in figure 8. The agreement between the theoretical and experi-
mental location is satisfactory near the tip of the cone and for some
distance downstream of the tip.[1]

The question of smooth shock-free supersonic-to-subsonic compres-
sion has been the subject of much discussion in recent years. The above
experimental results demonstrate that such a flow is possible. However,
the smooth compression is not of primary importance, but rather the con-
ditions under which it occurs. These conditions are that the sonic sur-
face bounds a zone of subsonic flow completely enclosed by a region of
supersonic flow and a solid surface.

[1]The existence of this type of flow is indicated by the experimental
results of Taylor and Maccoll (refs. 13 and 14) and was also discussed by
Tsien (ref. 23).

As an example of non-shock-free supersonic-to-subsonic compression, consider the flow past a two-dimensional airfoil at high subsonic speeds. The local supersonic zone on the airfoil is terminated by a shock wave and smooth compression through sonic velocity does not occur. In the two-dimensional case, however, the supersonic zone is bounded by a subsonic region and a solid surface. This is the opposite arrangement to that in the flow about a cone, in regime IV, where shock-free supersonic-to-subsonic compression does occur.

The above considerations illustrate that the existence (or stability) of shock-free compression through sonic velocity may not be a local phenomenon but may depend on the arrangement of the complete flow field.

Shock-Wave Angle

The angle of the attached shock wave at the nose of the cone was determined for a 20° and a 25° semiangle cone in flow regimes III, IV, and V. The values are shown in figure 9. Similar experiments are reported in references 13 and 14. Reference 22 presents data for one cone angle at one Mach number in regime III and one Mach number in regime IV. The agreement between the exact theory and the experimental values at the cone tip is very good even in regimes III and IV where the exact theory is not applicable for the complete finite cone.

Surface Mach Number Distribution

The distribution of the surface Mach number M_S on a 25° semiangle cone for various values of M_{∞} is shown in figure 10 and that on a 20° semiangle cone, in figure 11. Several characteristics of these distributions are of particular interest.

(1) Surface Mach number near the shoulder deviates from the Busemann conical values as soon as $M_S = 1.00$ is attained. Surface Mach number near the cone tip agrees quite well with the conical values until the theoretical detachment M_{∞} occurs. At the corner M_S should, except for boundary-layer effects, always be sonic if M_S forward of the shoulder is subsonic.

(2) As M_{∞} approaches 1.00 from the subsonic or from the supersonic regimes, M_S at a particular chordwise station approaches a constant value. This behavior implies that

$$\frac{dM_S}{dM_{\infty}}\bigg|_{M_{\infty}=1.00} = 0$$

The same behavior of M_s on two-dimensional sections was noted in reference 24, and thus the concept of stationary values of M_s at $M_\infty \doteq 1.00$ is established for two-dimensional and axially symmetric flow. Since these two cases represent limiting cases of the flow about general three-dimensional bodies, the stationary M_s concept can probably be applied quite generally if suitable care is taken in choosing the range of M_∞ about $M_\infty = 1.00$ in which the so-called "M_s freeze" is applicable.

(3) As M_∞ progresses from a subsonic value through $M_\infty = 1.00$ and on to a value in regime V, the M_s at a particular chordwise station probably varies quite smoothly with no abrupt variations, even at attachment of the shock wave, except for a region quite near the tip where large variations may occur when the shock wave attaches.

Drag Coefficients

The drag coefficients for the 20° and 25° semiangle cones are shown in figure 12. The values at $M_\infty = 1.00$ were determined by extrapolating the M_s data in figures 10 and 11 to $M_\infty = 1.00$.

Using the concept of stationary values of M_s at $M_\infty = 1.00$, the drag-curve slope at $M_\infty = 1.00$ becomes (see ref. 4 and appendix B)

$$\frac{dC_D}{dM_\infty}\bigg|_{M_\infty=1.00} = \frac{4}{\gamma + 1} - \frac{2}{\gamma + 1} C_D{}^* \tag{1}$$

where $C_D{}^*$ is the drag coefficient at $M_\infty = 1.00$. The first term $4/(\gamma + 1)$ of the drag-curve slope is derived from the first-order term of the pressure coefficient while the term $\left[2/(\gamma + 1)\right] C_D{}^*$ represents the contribution of the second-order terms. The magnitude of the second-order term $\left[2/(\gamma + 1)\right] C_D{}^*$ is shown by the difference in slope of the pairs of lines drawn through $C_D{}^*$ in figure 12.

The experimental results also indicate that

$$\frac{d^2 M_s}{dM_\infty{}^2}\bigg|_{M_\infty=1.00} = 0$$

This then implies (see appendix B) that

$$\frac{d^2C_D}{dM_\infty^2}\bigg|_{M_\infty=1.00} = -\frac{12\gamma + 4}{(\gamma + 1)^2} + \frac{10\gamma + 6}{(\gamma + 1)^2}\,C_D*$$

and an estimation can then be made of the range about $M_\infty = 1.00$ where equation (1) is valid.

Shock-Wave Detachment

Conical-flow theory indicates that for a given cone angle of a semi-infinite cone a certain minimum M_∞ is reached below which a conical solution is no longer possible. This value of M_∞ is defined to be the shock-wave detachment M_∞. However, a finite cone introduces a characteristic length into the problem so that curved attached shock waves, which would provide the necessary pressure gradient to turn the flow near the cone tip, may exist at values of M_∞ less than the conical detachment M_∞.

Present experimental results indicate only that shock-wave detachment for a given cone angle does not occur at an M_∞ greater than that predicted by conical theory. A collection of data from references 22, 25, 26, and 15 is shown in figure 13. The ratio δ/d where δ is the center-line distance from the shock wave to the plane of the cone shoulder and d is the body diameter at the shoulder, that is, the sonic point, is seen to approach asymptotically to the value of δ/d at attachment. The asymptotic behavior of δ/d complicates the fairing of the proper curve of δ/d versus M_∞ particularly in view of the paucity of experimental points in the immediate vicinity of shock-wave attachment.

In reference 27 data are presented for the shock-wave detachment distance of several cone angles at $M_\infty = 2.45$. A discrepancy was found between the experimental and theoretical values of the cone angle at which shock-wave detachment occurs for a fixed value of M_∞, detachment appearing to occur at a cone angle slightly greater than that predicted by the conical theory. This behavior would correspond to shock-wave detachment for a fixed cone angle occurring at a value of M_∞ less than the theoretical conical value of M_∞. Again, however, the discrepancy may be caused by the manner in which the experimental curve was faired.

Thus, the experimental results appear to indicate only that shock-wave detachment for a finite cone occurs at a value of M_∞ either less than or equal to the value of M_∞ predicted by conical theory but not

at a larger M_∞. The fact that shock-wave detachment does not appear
to occur at a value of M_∞ greater than that predicted by the conical
theory indicates that the presence of a boundary layer on the cone tip
does not affect the conicity of the flow near the cone tip to the extent
of precipitating detachment of the shock wave.

Figure 13 also indicates that when the shock-wave detachment dis-
tance is large, the position of the shock wave is dependent only on the
diameter of the cone at the shoulder or sonic point and is independent
of the cone angle. When the shock wave is quite near the cone tip, how-
ever, the detachment distance is also dependent on the cone angle. This
manner of behavior of the shock-wave separation distance was discussed
by Busemann (ref. 28) and was shown experimentally for two-dimensional
wedge sections by Griffith (ref. 29).

Transonic Similarity

The transonic-similarity rules for the drag coefficient and pres-
sure coefficient, as derived in reference 10, cannot be checked by the
experimental results of this report. The derivation assumes that the
cone-surface boundary condition is the approximate tangency condition
which is valid for relatively small angles. A 20° semiangle cone is
the minimum-angle cone for which detached shock-wave flow can be obtained
in the transonic wind tunnel, and thus the experimental models were 20°,
25°, and 30° semiangle cones. The experimental cone angles are much
larger than the cone angles for which the approximate tangency condition
is reasonable, and, therefore, the transonic-similarity rules of refer-
ence 10 are not applicable.

THEORETICAL CONSIDERATIONS

At the present time, theoretical solutions have not been found to
describe the flow about a finite cone for the complete Mach number range.
Theoretical solutions are available for only two Mach number regimes,
namely:

(1) Exact conical theory may be applied if the surface Mach number
    is greater than sonic

(2) At $M_\infty = 1.00$, Yoshihara (ref. 11) has calculated the flow about
    small-angle cones by a relaxation technique

No solution has been determined if M_∞ is less than sonic. How-
ever, Van Dyke's second-order supersonic theory and technique (ref. 30)

possibly can be applied to the subsonic case since, if the appropriate changes of sign are made in the particular solution found by Van Dyke for the supersonic case, the particular solution becomes valid for the subsonic case.

A solution remains to be found for the regime between $M_\infty = 1.00$ and the value of M_∞ where M_s becomes equal to 1.00. The problem would be greatly simplified if the transonic equations could be employed. To test the feasibility of the approximations inherent in the transonic equations, an approximate solution has been found for conical flow about a semi-infinite cone using the transonic equations. The details of the solution are presented in appendix C.

The solution is compared with the exact conical theory in figures 14 and 15. Figure 14 shows the comparison between the shock-wave angles predicted by the exact theory and by the transonic approximation. The surface Mach number comparison is shown in figure 15. From figure 15 it can be seen that the transonic approximation is quite satisfactory and is probably better than slender-body cone theory, since slender-body cone theory does not consider the presence of the conical shock wave. Also, figures 14 and 15 show the agreement of the cone angle at shock-wave detachment as found from the transonic solution and from the exact theory.

The above comparison of the exact conical solution and the approximate solution indicates that the transonic equations contain all the terms of importance in the exact equations for conical flow about cones, so that the transonic equations may be employed with confidence in the range of M_∞ from $M_\infty = 1.00$ to an M_∞ for which $M_s = 1.00$.

SUMMARY OF RESULTS

The following results were obtained from an investigation of transonic flow past cone cylinders.

1. The variation of drag coefficient C_D with free-stream Mach number M_∞ was determined experimentally. The slope of C_D versus M_∞ at $M_\infty = 1.00$ agrees with the theoretical prediction. The deviation of C_D versus M_∞ from the conical flow value of C_D when $M_s < 1.00$ is demonstrated.

2. The experimental results for the shock-wave angle, sonic-line location, and surface Mach number in the region near the cone tip indicate that the flow is conical near the tip of a finite cone even when the surface Mach number is less than sonic. The surface Mach numbers for the rest of the cone deviate from the exact conical values when

$M_S < 1.00$. Also, a case of shock-free supersonic-to-subsonic compression is demonstrated experimentally.

3. An approximate solution for transonic conical flow has been developed and the agreement with the exact conical theory indicates that the axially symmetric transonic equations retain the important features of the exact equations.

4. Present experimental values of the detachment distance of a shock wave from a finite cone tip do not demonstrate agreement with the detachment Mach number predicted by conical theory for a semi-infinite cone and the question of shock-wave detachment from a finite cone remains undecided.

California Institute of Technology,
     Pasadena, Calif., April 15, 1953.

P

APPENDIX A

REDUCTION OF INTERFEROMETER DATA

An interferometer determines the advancement or retardation of a light wave in a medium with respect to a coherent light wave in a reference medium. Since the wave velocities are a function of the indices of refraction of the respective mediums and consequently of the densities of the mediums, it may be shown that

$$dS = \frac{\kappa}{\lambda_0}\left[\rho(l) - \rho_R\right]dl \qquad (A1)$$

where

$\rho(l)$ density of undetermined medium

ρ_R density of reference medium

l path length

κ Gladstone-Dale constant

λ_0 wave length in vacuum of light employed

S   fringe shift; in case of finite-fringe interferograms this is ratio of displacement of a fringe to interval between undisturbed fringes

In equation (A1) it has been assumed that the light beams traverse identical geometrical paths, so that refraction, if present, is neglected. Also, the relationship between the index of refraction n and density is assumed to be

$$n = 1 + \kappa\rho \qquad (A2)$$

If $n = 1 + \alpha$ where $\alpha \ll 1$, equation (A2) is obtained by linearizing the Lorentz law.

For the axially symmetric case, the fringe shift for a light path perpendicular to the axis of symmetry becomes

$$S(y) = \frac{2\kappa}{\lambda_0}\int_y^\infty \frac{\left[\rho(r) - \rho_R\right]r\ dr}{\left(r^2 - y^2\right)^{1/2}}$$

where r is the radial distance from the axis of symmetry to a point on the light path and y is the perpendicular distance from the axis of symmetry to the light path.

In the present investigation, the density field was bounded by a shock wave at a distance y_s from the axis and the reference density was the free-stream density ρ_∞; thus,

$$S(y) = \frac{2\kappa}{\lambda_0} \int_y^{y_s} \frac{\left[\rho(r) - \rho_\infty\right] r \, dr}{\left(r^2 - y^2\right)^{1/2}} \tag{A3}$$

Weyl (ref. 31) introduced the assumption that $S(y)$ is a linear function of y^2 in a small interval of y. The validity of this assumption for the present investigation is indicated by the parabolic nature of the typical fringe-shift curves shown in figure 16. If the substitutions

$$v = r^2$$

$$u = y^2$$

$$u_s = y_s^2$$

are made, equation (A3) becomes

$$S(u) = \frac{\kappa}{\lambda_0} \int_u^{u_s} \frac{\left[\rho(v) - \rho_\infty\right] dv}{\sqrt{v - u}} \tag{A4}$$

This is analogous to the solution of Abel's problem. The solution of equation (A4) for ρ is

$$\rho(w) - \rho_\infty = -\frac{\lambda_0}{\pi} \int_w^{u_s} \frac{(dS/du) \, du}{\sqrt{u - w}} \tag{A5}$$

where $w = r^2$. A complete proof of the solution may be found in reference 19.

If the region of integration in equation (A5) is divided into equal increments in r of width b,

$$r_i = ib$$

where i is an integer. A numerical evaluation of equation (A5) is then

$$\frac{\rho(r_i)}{\rho_\infty} = 1 + \frac{2\lambda_0}{\pi \kappa a \rho_\infty} \sum_{k=i}^{N-1} \left(S_k - S_{k+1} \right) A_{ki} \qquad (A6)$$

where

$$r_s = Nb$$

and

$$A_{ki} = \frac{\sqrt{(k+1)^2 - i^2} - \sqrt{k^2 - i^2}}{2k + 1}$$

The above solution of the problem is essentially that of reference 18 and a table of A_{ki} for 50 intervals will be found in reference 18.

From the density ratio determined by equation (A6) the local Mach number may be computed. An approximate correction to the local stagnation pressure p_o' downstream of the shock wave was made by assuming that on the cone surface p_o' was determined by the nose shock-wave angle and at a given chordwise station p_o' varied linearly with the value on the shock wave at the given station. If the approximate stream-lines are calculated, as in reference 20, a more refined correction is obtained. From the experimental values of the local Mach number a topographic map was plotted, and from this map the desired Mach number contours are found.

Conical Fields

If it is desired to determine whether or not a given axially symmetric field is conical, a simple test can be made. Returning to equation (A3) it is assumed that

$$\rho = \rho(\eta)$$

where $\eta = r/x$ and x is the axial distance from the conical origin. Then equation (A3) becomes

$$\frac{S(y)}{x} = \frac{2\kappa}{\lambda_o} \int_{\eta_1}^{\eta_s} \frac{\left[\rho(\eta) - \rho_\infty\right] \eta \, d\eta}{\left(\eta^2 - \eta_1^2\right)^{1/2}}$$

where η_s is the tangent of the shock-wave angle and $\eta_1 = y/x$. Thus, if the field is truly conical,

$$\frac{S(y)}{x} = f\left(\frac{y}{x}\right)$$

and a plot of $S(y)/x$ versus y/x for various values of x will yield a group of coincident curves. Examples of this technique are shown in references 19 and 20. It is interesting to note that in reference 20 figure 6(b) indicates conical flow near a cone tip for flow regime IV, that is, a $35°$ semiangle cone at $M_\infty = 1.87$, using the above technique.

Subsidiary Considerations

Model size.- From equation (A3) it is evident that the fringe shift at a particular chordwise and radial station is a linear function of the model size for fixed values of density. Thus the model should be as large as is compatible with the test-section dimensions with regard to blocking and so forth.

Finite fringe spacing.- The fringe spacing in the undisturbed field must be such that a sufficient number of data points may be determined between the shock wave and the cone surface at a particular chordwise station. However, for a given fringe shift S the displacement of the fringe is proportional to the undisturbed fringe spacing, and the accuracy of the fringe data will be improved by increasing the undisturbed spacing. A compromise must be effected between the desire for many fringe shift points at a given chordwise station and the accuracy of the individual points. In the present investigation, this compromise precluded a study by interferometry of the flow properties in the immediate vicinity of the cone tip when the shock wave was attached.

Accuracy.- The accuracy of the interferometric method is affected by refraction, inhomogeneities in the reference flow, the numerical approximation, and so forth. An estimate of the accuracy can be obtained by noting the comparison of interferometer data and shock-reflection data

in figure 3 and the values of local Mach number behind the shock wave indicated in figures 6 and 7.

Comprehensive discussions of the accuracy of the method may be found in references 18 and 19.

APPENDIX B

VARIATION OF PRESSURE AND DRAG COEFFICIENTS NEAR $M_\infty = 1.00$

The pressure coefficient

$$C_p = \frac{2}{\gamma M_\infty^2}\left(\frac{p_s}{p_\infty} - 1\right)$$

where p_s is the surface static pressure and p_∞ is the free-stream static pressure may, in transonic flow, be written as

$$C_p = \frac{2}{\gamma M_\infty^2}\left[\left(\frac{1 + \frac{\gamma - 1}{2}M_\infty^2}{1 + \frac{\gamma - 1}{2}M_s^2}\right)^{\gamma/(\gamma-1)} - 1\right] \qquad (B1)$$

where M_s is the surface Mach number. In equation (B1) it has been assumed that

$$\frac{\Delta p_o}{p_o} \approx O\left(M^2 - 1\right)^3$$

that is, the stagnation pressure loss across any shock waves may be neglected.

Defining ζ and ξ as

$$\zeta = M_\infty^2$$

$$\xi = M_s^2$$

Equation (B1) becomes

$$C_p = f(\zeta,\xi) = \frac{2}{\gamma\zeta}\left[\left(\frac{1 + \frac{\gamma - 1}{2}\zeta}{1 + \frac{\gamma - 1}{2}\xi}\right)^{\gamma/(\gamma-1)} - 1\right] \qquad (B2)$$

For a fixed body geometry, M_s is a function of M_∞ only, therefore

$$\xi = \xi(\zeta)$$

Thus, the first and second total derivatives of C_p with respect to ζ are

$$\frac{dC_p}{d\zeta} = f_\zeta + f_\xi \frac{d\xi}{d\zeta} \tag{B3}$$

and

$$\frac{d^2C_p}{d\zeta^2} = f_{\zeta\zeta} + 2f_{\zeta\xi} \frac{d\xi}{d\zeta} + f_{\xi\xi} \left(\frac{d\xi}{d\zeta}\right)^2 + f_\xi \frac{d^2\xi}{d\zeta^2} \tag{B4}$$

In general, $d\xi/d\zeta$ and $d^2\xi/d\zeta^2$ are not known; however, an argument presented by Liepmann and Bryson (ref. 24) shows that, for $\zeta = 1.00$, $d\xi/d\zeta = 0$. The same argument, namely, that M_s has a stationary value at $M_\infty = 1.00$, cannot be used to evaluate $d^2\xi/d\zeta^2$. However, an inspection of the experimental data (see figs. 10 and 11) indicates that the curve of M_s versus M_∞ has an inflection point at $M_\infty = 1.00$ and, thus, $d^2\xi/d\zeta^2 = 0$ at $\zeta = 1.00$.

Using equations (B3) and (B4) and the above argument, the derivatives of C_p become

$$\left(\frac{dC_p}{d\zeta}\right)^* = f_\zeta^*$$

$$\left(\frac{d^2C_p}{d\zeta^2}\right)^* = f_{\zeta\zeta}^*$$

where ( )* indicates evaluation at $\zeta = 1.00$, that is, at $M_\infty = 1.00$. The derivatives of C_p with respect to M_∞ are then

$$\left(\frac{dC_p}{dM_\infty}\right)^* = 2f_\zeta^*$$

$$\left(\frac{d^2C_p}{dM_\infty^2}\right)^* = 4f_{\zeta\zeta}^* + 2f_\zeta^*$$

The partial derivatives $f_{\zeta\zeta}$ and f_{ζ} may be calculated from equation (B2) and thus

$$\left(\frac{dC_p}{dM_\infty}\right)^* = \frac{4}{\gamma + 1} - \frac{2}{\gamma + 1} C_p^* \tag{B5}$$

$$\left(\frac{d^2C_p}{dM_\infty^2}\right)^* = -\frac{12\gamma + 4}{(\gamma + 1)^2} + \frac{10\gamma + 6}{(\gamma + 1)^2} C_p^* \tag{B6}$$

The fore drag coefficient of a finite cone is given by

$$C_D = \int_0^1 C_p(\alpha) \, d\alpha$$

where $\alpha = \left(r/r_b\right)^2$, r is the local cone radius, and r_b is the cone base radius. Using equations (B5) and (B6), the derivatives of C_D are

$$\left(\frac{dC_D}{dM_\infty}\right)^* = \frac{4}{\gamma + 1} - \frac{2}{\gamma + 1} C_D^* \tag{B7}$$

and

$$\left(\frac{d^2C_D}{dM_\infty^2}\right)^* = -\frac{12\gamma + 4}{(\gamma + 1)^2} + \frac{10\gamma + 6}{(\gamma + 1)^2} C_D^* \tag{B8}$$

A comparison of equation (B7) and experimental data is shown in figure 12. Equations (B5) and (B7) were given previously by Bryson (ref. 4).

It should be noted that the first term $4/(\gamma + 1)$ of equation (B5) may be derived from the linearized transonic C_p (ref. 1) which is

$$C_p = 2 \frac{M_\infty^2 - M_s^2}{(\gamma + 1)} \tag{B9}$$

The second term $-\left[2/(\gamma + 1)\right] C_p^*$ of equation (B5) is then of the nature of a second-order correction term. However, if $\left(d^2 C_p/dM_\infty^2\right)^*$ is computed from equation (B9), the result does not agree with the first term of equation (B6) and is, in fact, of opposite sign.

APPENDIX C

TRANSONIC APPROXIMATION FOR CONICAL FLOW

In discussing axially symmetric transonic flow, the following approximations to the exact equations and boundary conditions are employed.

If q_x is the velocity in the axial or X-direction and q_r is the velocity in the radial or r-direction it is assumed that

$$q_x = a^* + \phi_x$$

$$q_r = \phi_r$$

where a^* is the velocity of sound at $M_\infty = 1.00$, ϕ is the perturbation potential, and ϕ_x, $\phi_r \ll a^*$. Then, defining

$$u = \frac{\gamma + 1}{a^*} \phi_x$$

$$v = \frac{\gamma + 1}{a^*} \phi_r$$

the continuity equation is approximated by

$$u u_x - v_r - \frac{1}{r} v = 0 \qquad (C1)$$

and the condition of irrotationality becomes

$$u_r - v_x = 0 \qquad (C2)$$

The exact tangency condition on the body surface is replaced by

$$v_o = (\gamma + 1) \tan \theta \qquad (C3)$$

where v_o is v on the surface of the body and θ is the inclination angle of the body surface. The above relations are derived in greater detail in reference 9.

To test the feasibility of the approximations inherent in equations (C1), (C2), and (C3) an approximate solution for the flow about a semi-infinite cone will be developed. This approximation will then be compared with the Busemann solution of the exact equations.

Conical Solution

Assuming that u and v are functions of σ where

$$\sigma = \frac{x}{r}$$

equations (C1) and (C2) become

$$uu_\sigma + \sigma v_\sigma - v = 0 \qquad \text{(C1a)}$$

$$\sigma u_\sigma + v_\sigma = 0 \qquad \text{(C2a)}$$

A solution of the form

$$u = f(v) \qquad \text{(C4)}$$

will be sought. From equation (C4)

$$\frac{du}{d\sigma} = \frac{du}{dv}\frac{dv}{d\sigma}$$

but from equation (C2a)

$$\frac{dv}{d\sigma} = -\sigma\frac{du}{d\sigma}$$

Therefore

$$\frac{du}{dv} = -\frac{1}{\sigma} \tag{C5}$$

The relationship in equation (C5) is exact (see ref. 32).

Differentiating equation (C5) with respect to σ yields

$$\frac{dv}{d\sigma} = \frac{1}{\sigma^2 \dfrac{d^2u}{dv^2}} \tag{C6}$$

and therefore

$$\frac{du}{d\sigma} = -\frac{1}{\sigma^3 \dfrac{d^2u}{dv^2}} \tag{C7}$$

Substituting equations (C5), (C6), and (C7) into equation (C1a), the result is

$$v\frac{d^2u}{dv^2} + \frac{du}{dv} = u\left(\frac{du}{dv}\right)^3 \tag{C8}$$

The following conditions are imposed on equation (C8).

(a) At the shock wave: If u_s and v_s are the values of u and v at the shock wave, then, from the transonic-shock polar relation,

$$v_s = \left(u_\infty - u_s\right)\sqrt{\frac{u_\infty + u_s}{2}} \tag{C9}$$

where

$$u_\infty = M_\infty^2 - 1$$

The shock-wave angle β is given by

$$\cot\beta = \frac{v_s}{u_\infty - u_s}$$

hence, from equation (C5),

$$\frac{du}{dv}\bigg|_s = -\frac{u_\infty - u_s}{v_s} \qquad (C10)$$

(b) On the Cone Surface: The tangency condition must be satisfied, hence

$$v_o = (\gamma + 1) \tan \theta \qquad (C11)$$

where v_o is v on the cone surface and θ is the cone semiangle. From equation (C5)

$$\frac{du}{dv}\bigg|_o = -\tan \theta \qquad (C12)$$

An exact solution of equation (C8) has not been found. However, if the right-hand side of equation (C8) is assumed to be small, an iteration solution may be found.

First Approximation

As a first approximation to the solution, set the right-hand side of equation (C8) equal to zero; that is,

$$\frac{d}{dv}\left(v \frac{du}{dv}\right) = 0 \qquad (C13)$$

The solution of equation (C13) is

$$u = A \log_e Bv \qquad (C14)$$

Applying conditions (C9) and (C10) to this solution, equation (C14) becomes

$$u = u_s - \left(u_\infty - u_s\right) \log_e \frac{v}{v_s} \qquad (C15)$$

Second Approximation

As a second approximation to the solution of equation (C8), the right-hand side of equation (C8) is assumed to be given with sufficient accuracy by equation (C15). Hence

$$\frac{d}{dv}\left(v\,\frac{du}{dv}\right) = -\frac{u_s\left(u_\infty - u_s\right)^3}{v^3} + \frac{\left(u_\infty - u_s\right)^4}{v^3}\,\log_e\frac{v}{v_s} \qquad (C16)$$

The solution of equation (C16) is

$$u = \frac{\left(u_\infty - u_s\right)^3}{4v^2}\left[-u_s + \left(u_\infty - u_s\right) + \left(u_\infty - u_s\right)\log_e\frac{v}{v_s}\right] + C\,\log_e Dv \qquad (C17)$$

Applying conditions (C9) and (C10) to this solution, equation (C17) becomes

$$u = \frac{\left(u_\infty - u_s\right)^3}{4v^2}\left[-u_s + \left(u_\infty - u_s\right) + \left(u_\infty - u_s\right)\log_e\frac{v}{v_s}\right] -$$

$$\frac{\left(u_\infty + 5u_s\right)\left(u_\infty - u_s\right)}{2\left(u_\infty + u_s\right)}\,\log_e\frac{v}{v_s} - \frac{u_\infty\left(u_\infty - 5u_s\right)}{2\left(u_\infty + u_s\right)} \qquad (C18)$$

The values of u_s and v_s appearing in equation (C18) are not independent of the cone semiangle θ. Applying condition (C12) to equation (C18) and solving for v_s, the result is

$$\log_e v_s = \log_e\left(\gamma + 1\right)\tan\theta + \frac{\left[\left(\gamma + 1\right)\tan\theta\right]^2\left(u_\infty + 5u_s\right)}{\left(u_\infty + u_s\right)\left(u_\infty - u_s\right)^3} -$$

$$\left(\frac{u_s}{u_\infty - u_s} - \frac{1}{2}\right) - \frac{2(\gamma + 1)^3\tan^4\theta}{\left(u_\infty - u_s\right)^4} \qquad (C19)$$

The transonic-shock polar relation also must be satisfied, hence

$$v_S = \left(u_\infty - u_S\right) \sqrt{\frac{u_\infty + u_S}{2}} \tag{C20}$$

Because of the nature of equation (C19), explicit solutions of equations (C19) and (C20) for u_S and v_S in terms of u_∞ and θ have not been found. However, a solution may be found graphically.

The values of u_S and v_S thus determined for a given value of θ and u_∞ may be introduced into equation (C18). If the value of u on the surface u_O is desired, then substitution of

$$v = v_O = (\gamma + 1) \tan \theta$$

in equation (C18) yields u_O.

It should be noted that, for a given value of θ and u_∞, two sets of values for u_S and v_S are found. These correspond to the "strong" and "weak" shock waves.

Comparison of Second Approximation and Busemann Conical Solution

<u>Wave angle</u>.- The wave angle β is determined by the values of u_S and v_S since

$$\cot \beta = \frac{v_S}{u_\infty - u_S}$$

The degree of agreement is apparent in figure 14.

<u>Surface Mach number</u>.- In terms of u_O and v_O, the surface Mach number is

$$M_S{}^2 = \frac{2}{\gamma + 1} A \left(\frac{1}{1 - \dfrac{\gamma - 1}{\gamma + 1} A}\right) \tag{C21}$$

where

$$A = \left(1 + \frac{u_O}{\gamma + 1}\right)^2 + \left(\frac{v_O}{\gamma + 1}\right)^2$$

The usual transonic approximation reduces equation (C21) to

$$M_s{}^2 = 1 + u_0 \qquad\qquad (C22)$$

equation (C21) is shown in figure 15. The agreement with the exact theory is quite satisfactory.

Apple curve.- Two sets of values of u_s and v_s will satisfy equations (C19) and (C20). The two solutions correspond to the "strong" and "weak" shock-wave solutions predicted by Busemann. If the values of u_0 and v_0 for all possible cone angles and for both types of solution are plotted in the hodograph, the resultant curve is Busemann's "apple" curve. The apple curve found in the second approximation is shown in figure 17.

REFERENCES

1. Cole, J. D.: Drag of a Finite Wedge at High Subsonic Speeds. Jour. Math. and Phys., vol. 30, no. 2, July 1951, pp. 79-93.

2. Guderley, Gottfried, and Yoshihara, Hideo: The Flow Over a Wedge Profile at Mach Number One. Tech. Rep. No. 5783, Air Materiel Command, Army Air Forces, July 1949.

3. Vincenti, Walter G., and Wagoner, Cleo B.: Transonic Flow Past a Wedge Profile With Detached Bow Wave. NACA Rep. 1095, 1952. (Supersedes NACA TN 2339 and TN 2588.)

4. Bryson, Arthur Earl, Jr.: An Experimental Investigation of Transonic Flow Past Two-Dimensional Wedge and Circular-Arc Sections Using a Mach-Zehnder Interferometer. NACA Rep. 1094, 1951. (Supersedes NACA TN 2560.)

5. Griffith, Wayland: Shock-Tube Studies of Transonic Flow Over Wedge Profiles. Jour. Aero. Sci., vol. 19, no. 4, Apr. 1952, pp. 249-257.

6. Vincenti, Walter G., and Wagoner, Cleo B.: Theoretical Study of the Transonic Lift of a Double-Wedge Profile With Detached Bow Wave. NACA TN 2832, 1952.

7. Guderley, Gottfried, and Yoshihara, Hideo: Two-Dimensional Unsymmetric Flow Patterns at Mach Number One. WADC TR 6683, Jan. 1952.

8. Cole, J. D., Solomon, G. E., and Willmarth, W. W.: Transonic Flow Past Simple Bodies. Jour. Aero. Sci., vol. 20, no. 9, Sept. 1953, pp. 627-634.

9. Von Kármán, Theodor: The Similarity Law of Transonic Flow. Jour. Math. and Phys., vol. 26, no. 3, Oct. 1947, pp. 182-190.

10. Oswatitsch, K., and Berndt, S. B.: Aerodynamic Similarity at Axisymmetric Transonic Flow Around Slender Bodies. Aero. TN 15, Roy. Inst. Tech., Sweden, May 11, 1950.

11. Yoshihara, H.: On the Flow Over a Cone-Cylinder Body at Mach Number One. WADC TR 52-295, Nov. 1952.

12. Busemann, A.: Drücke auf kegelförmige Spitzen bei Bewegung mit Überschallgeschwindigkeit. Z.a.M.M., Bd. 9, Heft 6, Dec. 1929, pp. 496-498.

13. Taylor, G. I., and Maccoll, J. W.: The Air Pressure on a Cone Moving at High Speeds. Proc. Roy. Soc. (London), ser. A, vol. 139, no. 838, Feb. 1, 1933, pp. 278-311.

14. Maccoll, J. W.: The Conical Shock Wave Formed by a Cone Moving at a High Speed. Proc. Roy. Soc. (London), ser. A, vol. 159, no. 898, Apr. 1, 1937, pp. 459-472.

15. Drougge, G.: The Flow Around Conical Tips in the Upper Transonic Range. Rep. No. 25, The Aero. Res. Inst. of Sweden (Stockholm), 1948.

16. Dhawan, Satish, and Roshko, Anatol: A Flexible Nozzle for a Small Supersonic Wind Tunnel. Jour. Aero. Sci., vol. 18, no. 4, Apr. 1951, pp. 253-258.

17. Ashkenas, Harry I., and Bryson, Arthur E.: Design and Performance of a Simple Interferometer for Wind-Tunnel Measurements. Jour. Aero. Sci., vol. 18, no. 2, Feb. 1951, pp. 82-90.

18. Gooderum, Paul B., and Wood, George P.: Density Fields Around a Sphere at Mach Numbers 1.30 and 1.62. NACA TN 2173, 1950.

19. Bennett, F. D., Carter, W. C., and Bergdolt, V. E.: Interferometric Analysis of Airflow About Projectiles in Free Flight. Jour. Appl. Phys., vol. 23, no. 4, Apr. 1952, pp. 453-469.

20. Bergdolt, V. E.: Air Flow About Cone Cylinders With Curved Shock Waves. Rep. No. 832, Ballistic Res. Lab. (Aberdeen, Md.), Sept. 1952.

21. Liepmann, H. W., and Ashkenas, H.: Shock-Wave Oscillations in Wind Tunnels. Jour. Aero. Sci., vol. 14, no. 5, May 1947, pp. 295-302.

22. Muirhead, Vincent U.: Flow Field Around a Finite Cone With Shock. A.E. Thesis, C.I.T., 1949.

23. Tsien, Hsue-shen: The "Limiting Line" in Mixed Subsonic and Super- sonic Flow of Compressible Fluids. NACA TN 961, 1944.

24. Liepmann, H. W., and Bryson, A. E., Jr.: Transonic Flow Past Wedge Sections. Jour. Aero. Sci., vol. 17, no. 12, Dec. 1950, pp. 745-755.

25. Marschner, B. W.: An Investigation of Detached Shock Waves. A.E. Thesis, C.I.T., 1948.

26. Heberle, Juergen W., Wood, George P., and Gooderum, Paul B.: Data on Shape and Location of Detached Shock Waves on Cones and Spheres. NACA TN 2000, 1950.

27. Johnston, G. W.: An Investigation of the Flow About Cones and Wedges at and Beyond the Critical Angle. Rep. No. 24, Inst. Aerophys., Univ. of Toronto, Dec. 1952.

28. Busemann, Adolf: A Review of Analytical Methods for the Treatment of Flows With Detached Shocks. NACA TN 1858, 1949.

29. Griffith, Wayland C.: Transonic Flow. Tech. Rep. II-7, Contract N6ori-105, Task II, Project NR061-020, Office of Naval Res. and Dept. Phys., Princeton Univ., Dec. 19, 1950.

30. Van Dyke, Milton D.: A Study of Second-Order Supersonic-Flow Theory. NACA Rep. 1081, 1952. (Supersedes NACA TN 2200.)

31. Weyl, F. Joachim: Analytical Methods in Optical Examination of Supersonic Flow. Rep. 211-45, Bur. Ord, Navy Dept., Dec. 11, 1945.

32. Ferri, A.: Elements of Aerodynamics of Supersonic Flows. The Macmillan Co., 1949.
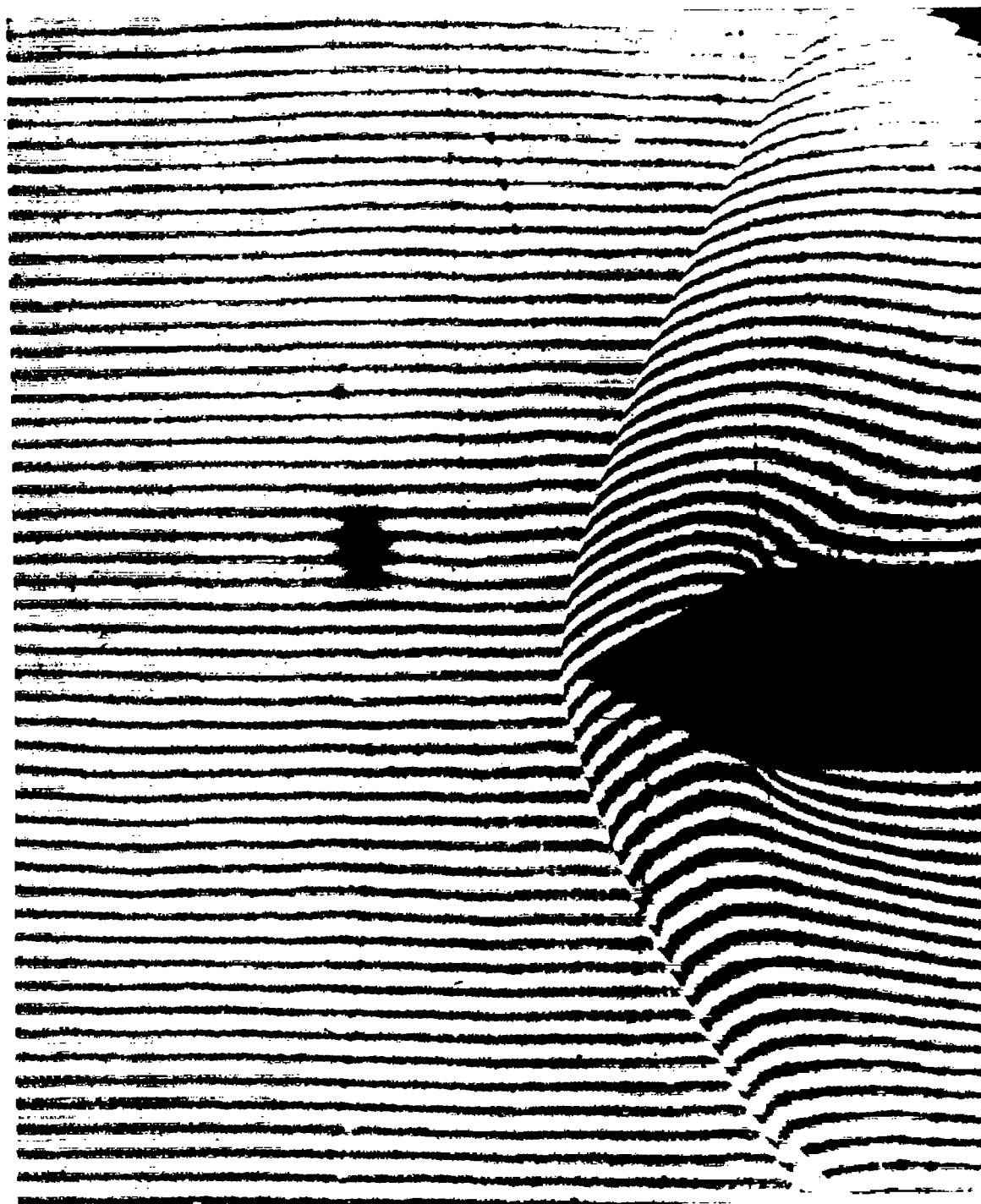
L-84893
Figure 1.- Finite-fringe interferogram for 30° semiangle cone cylinder.
$M_\infty = 1.280$.
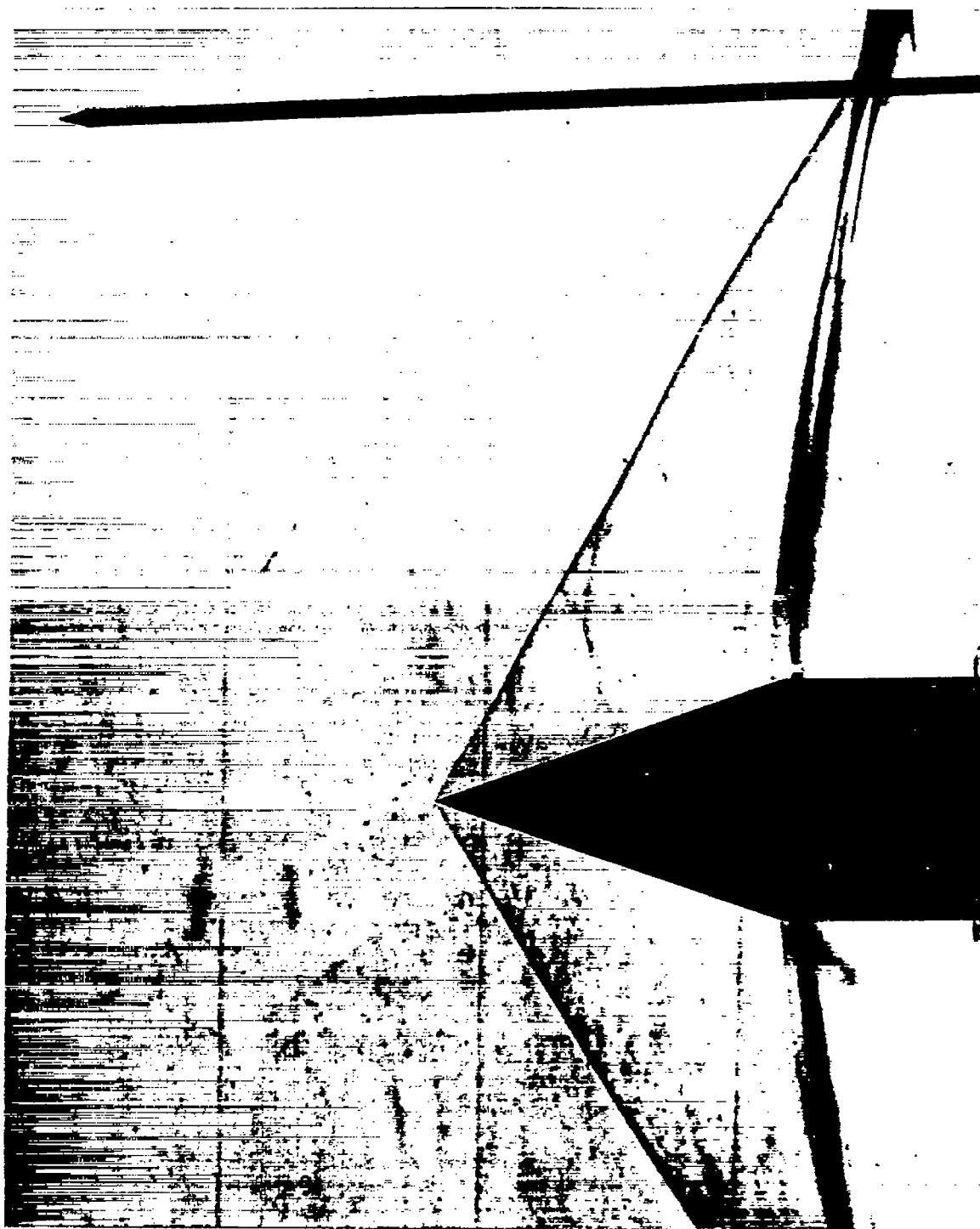
L-84894

Figure 2.- Wave reflection from sonic line for 20° semiangle cone cylinder.
$M_\infty = 1.297$.
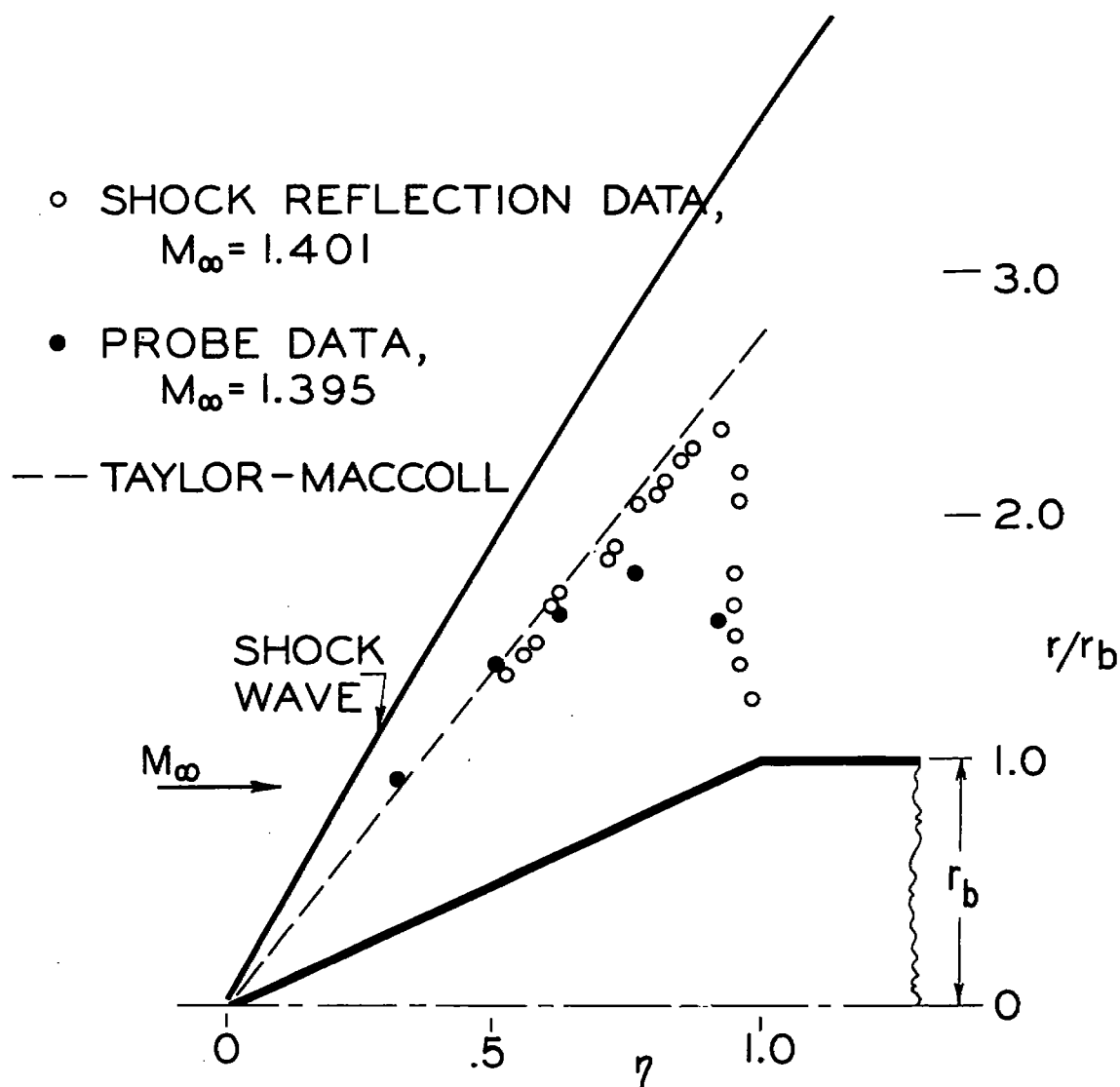
Figure 3.- Sonic-line location for 25° semiangle cone cylinder.
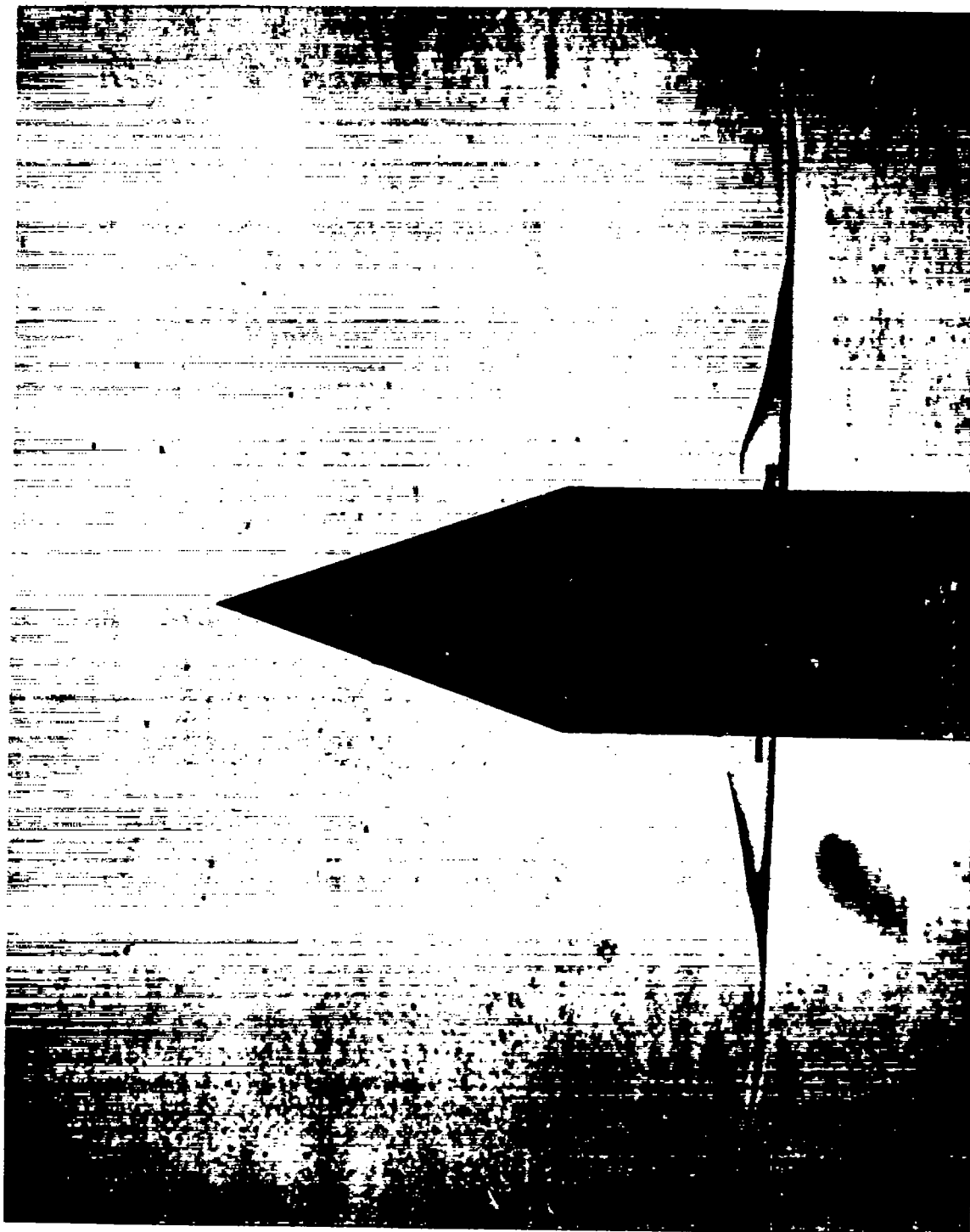
L-84895

Figure 4.- 20° semiangle cone cylinder. $M_\infty = 0.942$.
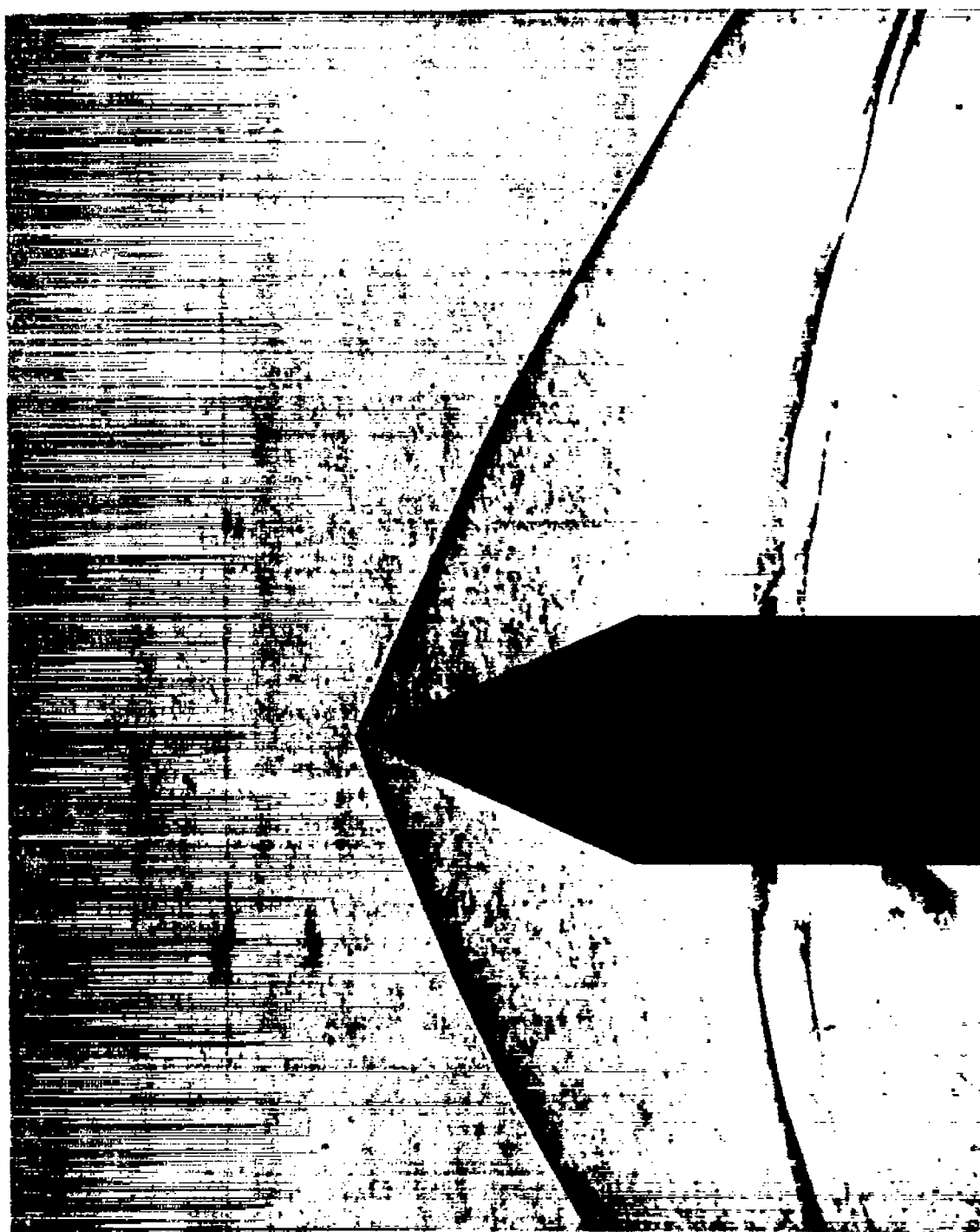
(a) $M_\infty = 1.328$.

Figure 5.- 25° semiangle cone cylinder.
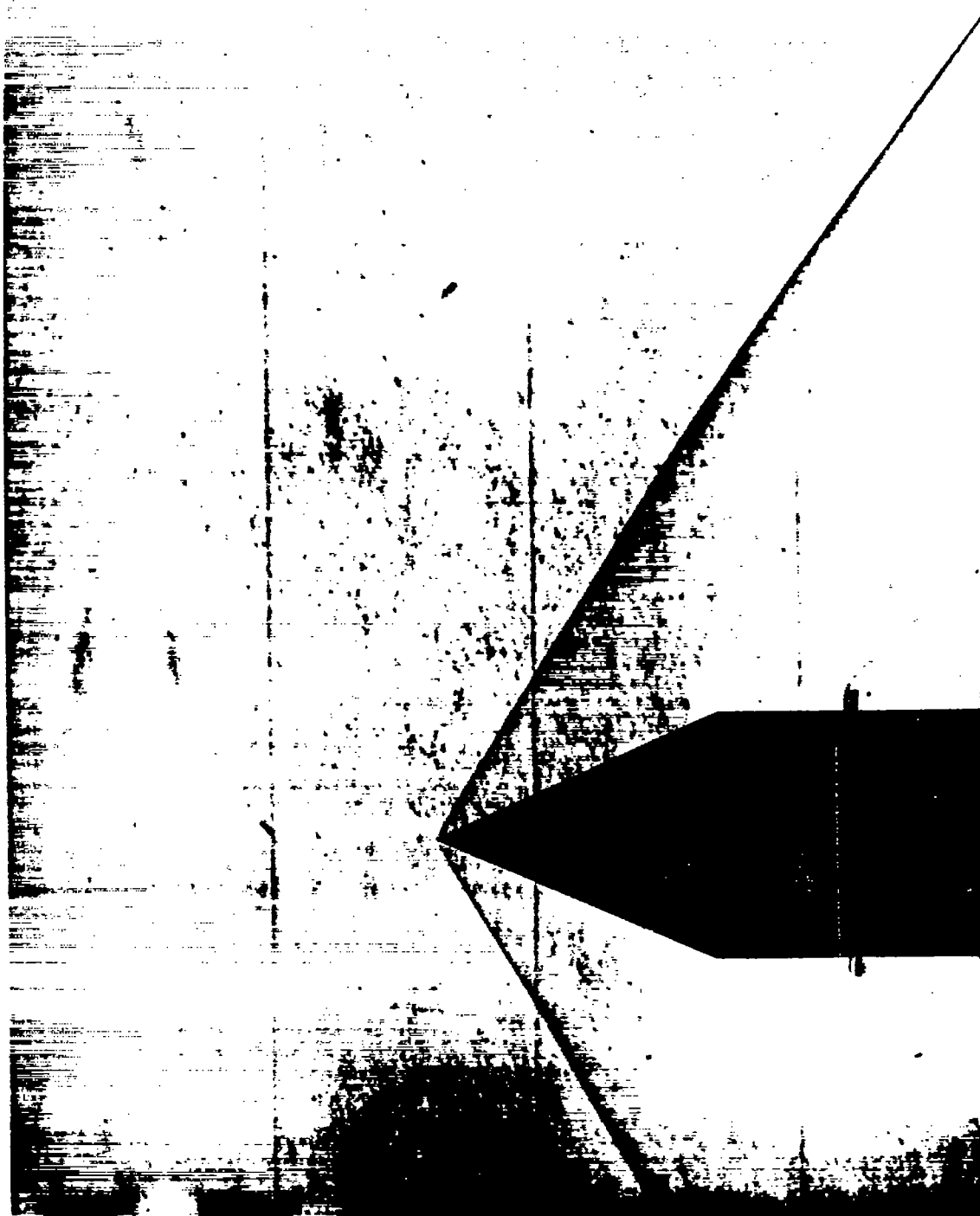
(b) $M_\infty = 1.415$.

L-84897

Figure 5.- Concluded.
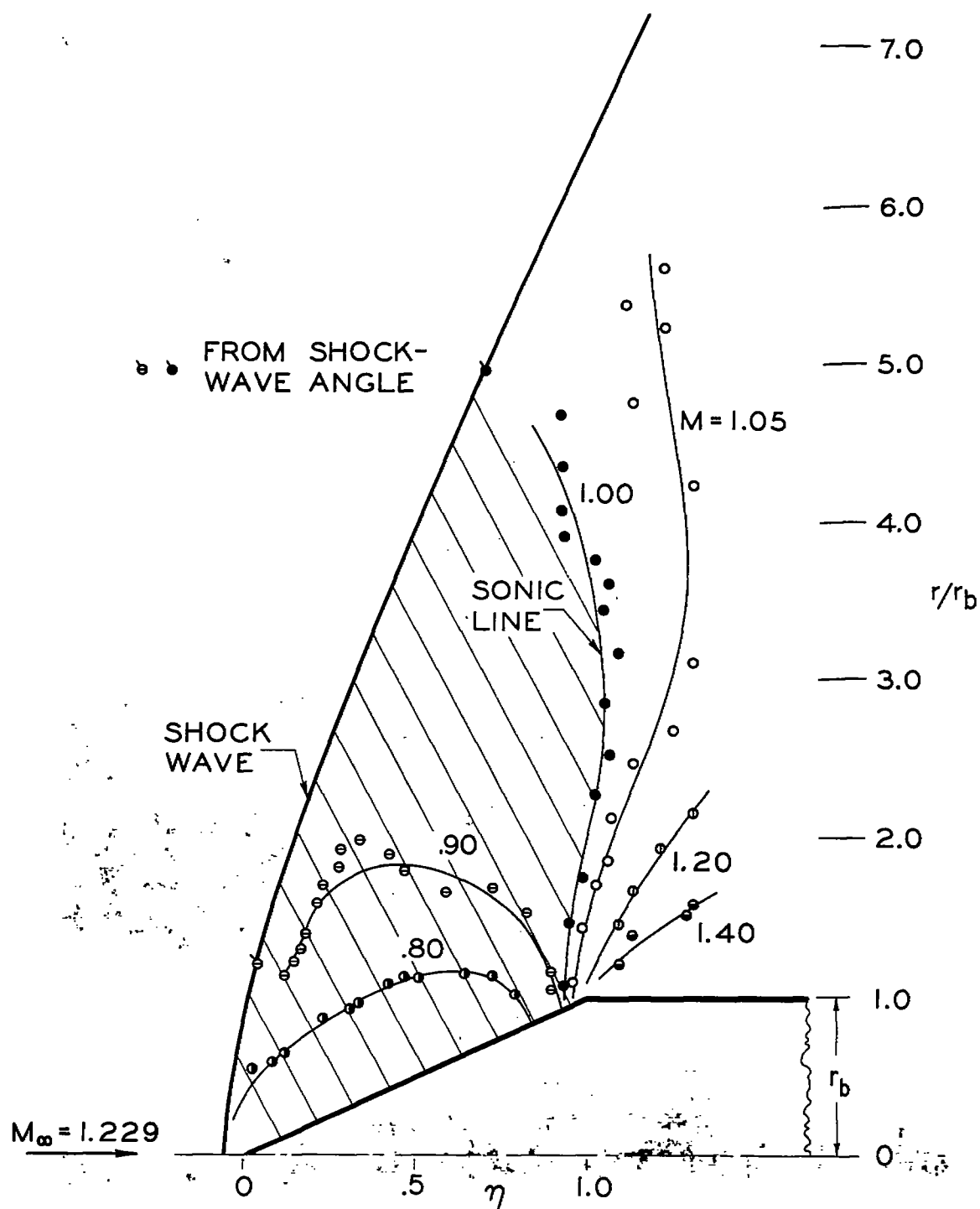
(a) $M_\infty = 1.229$.

Figure 6.- Mach number field for $25°$ semiangle cone cylinder.

FROM SHOCK-
WAVE ANGLE

M=1.10

SONIC
LINE

1.00

SHOCK
WAVE

.90

1.20

.80

1.40

.70

$M_\infty = 1.253$

r/r_b

7.0

6.0

5.0

4.0

3.0

2.0

1.0

r_b

0

0   .5   1.0

η
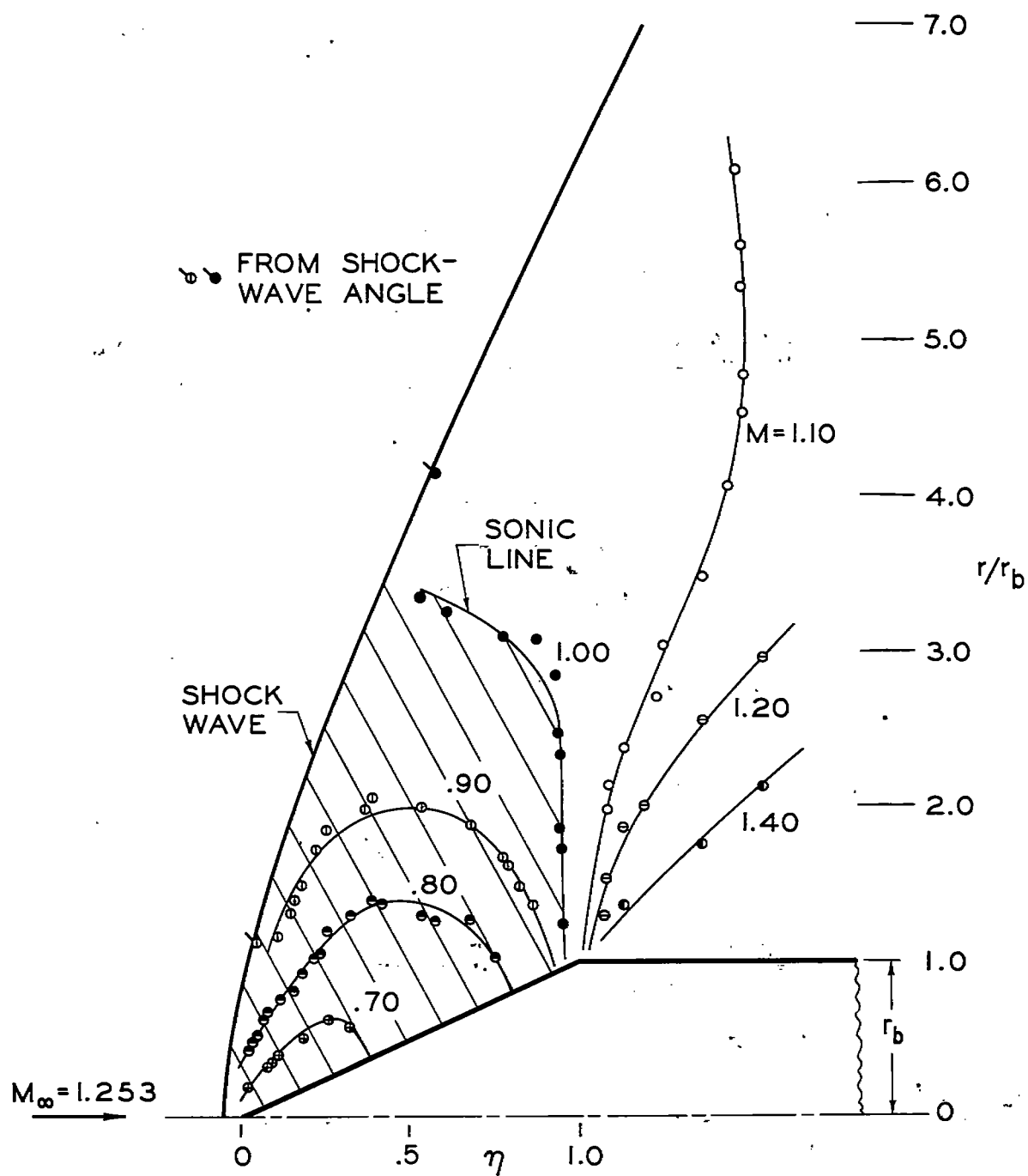
(b) $M_\infty = 1.253$.
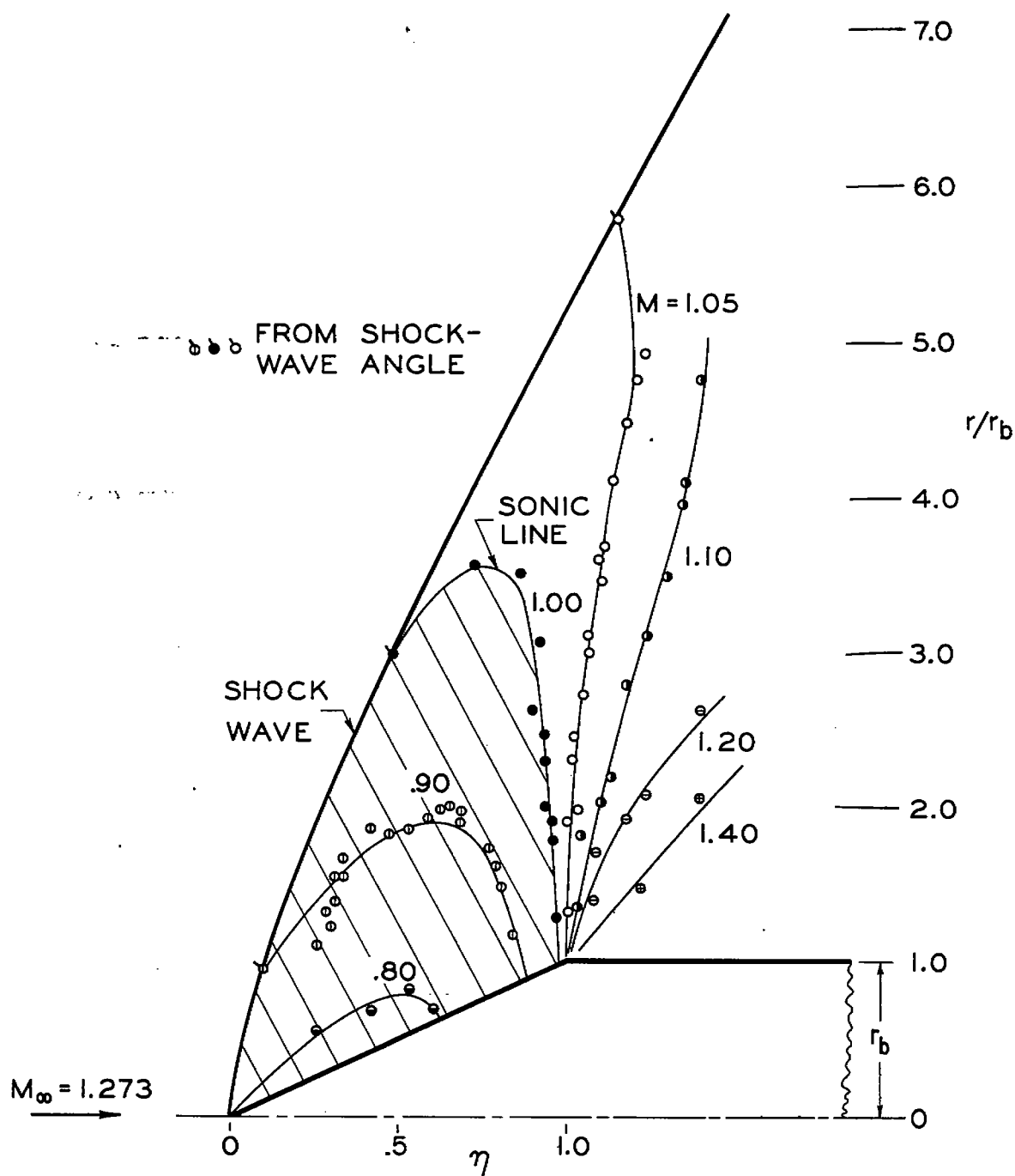
Figure 6.- Continued.

(c) $M_\infty = 1.273$.

Figure 6.- Continued.
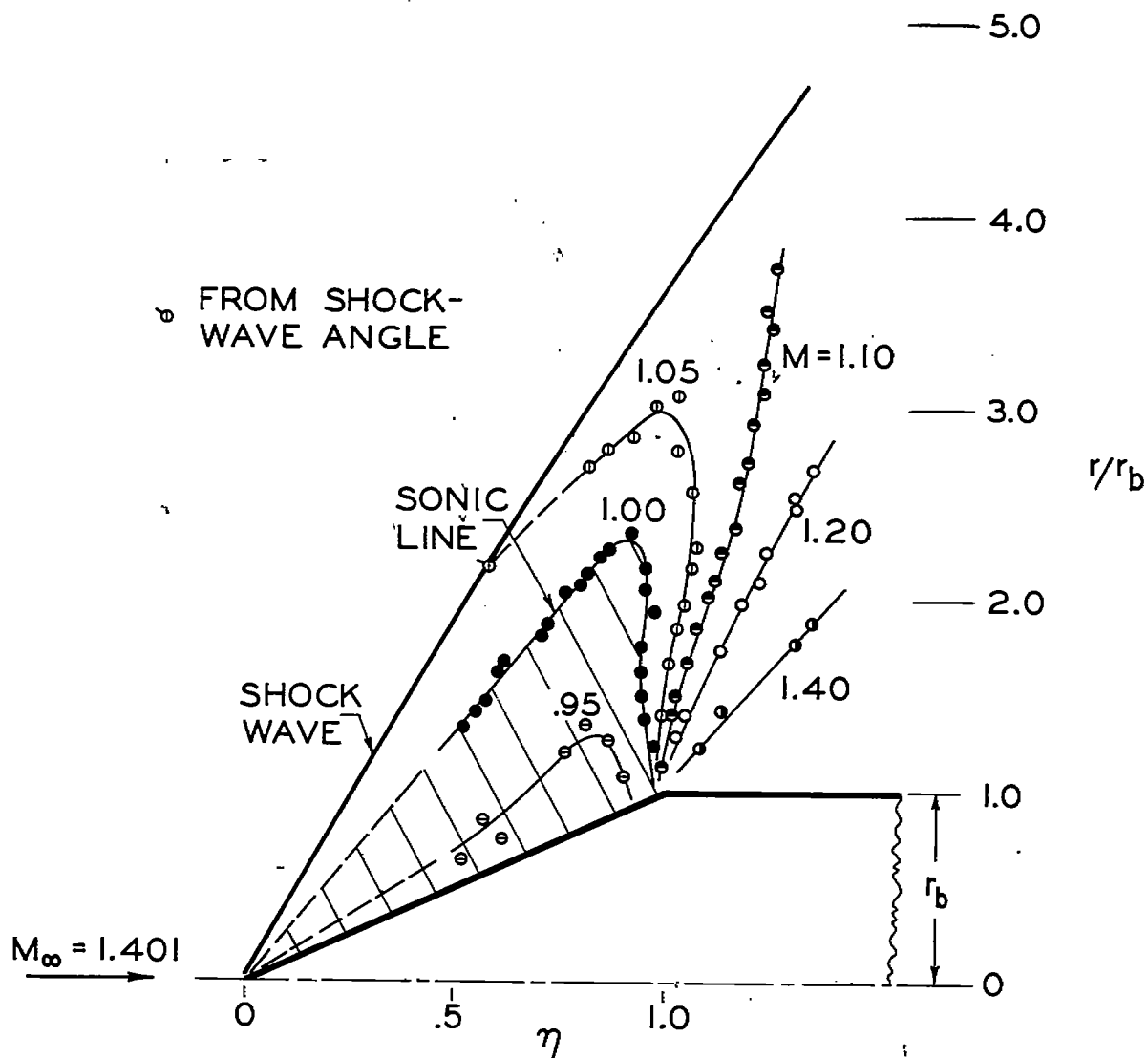
(d) $M_\infty = 1.401$.

Figure 6.- Concluded.

Figure 7.- Mach number field for 30° semiangle cone cylinder.
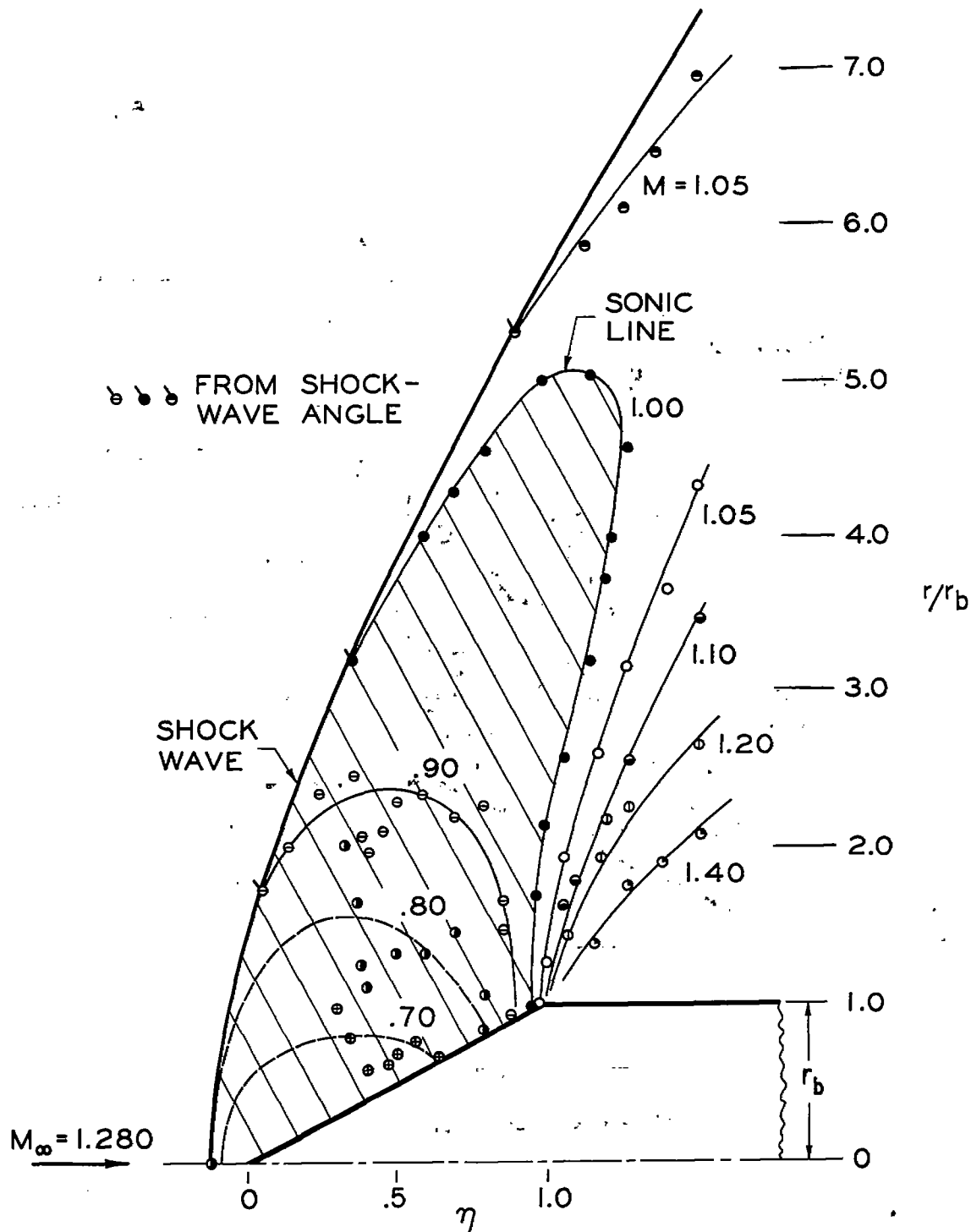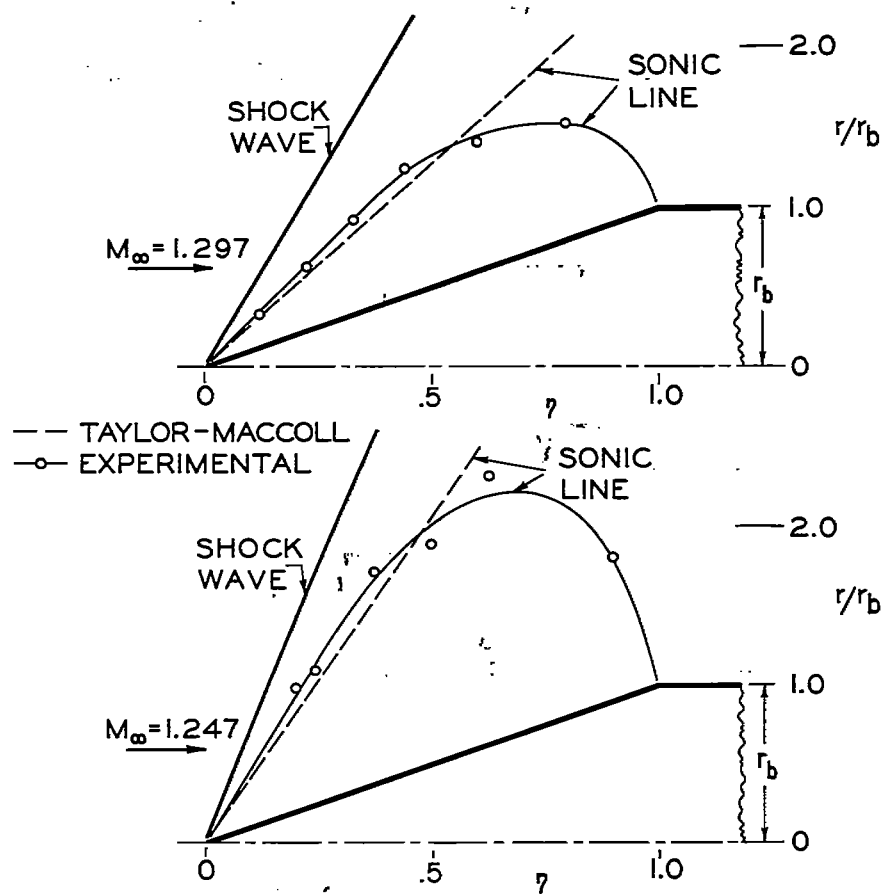
Figure 8.- Sonic-line location by shock reflection for 20° semiangle cone cylinder.
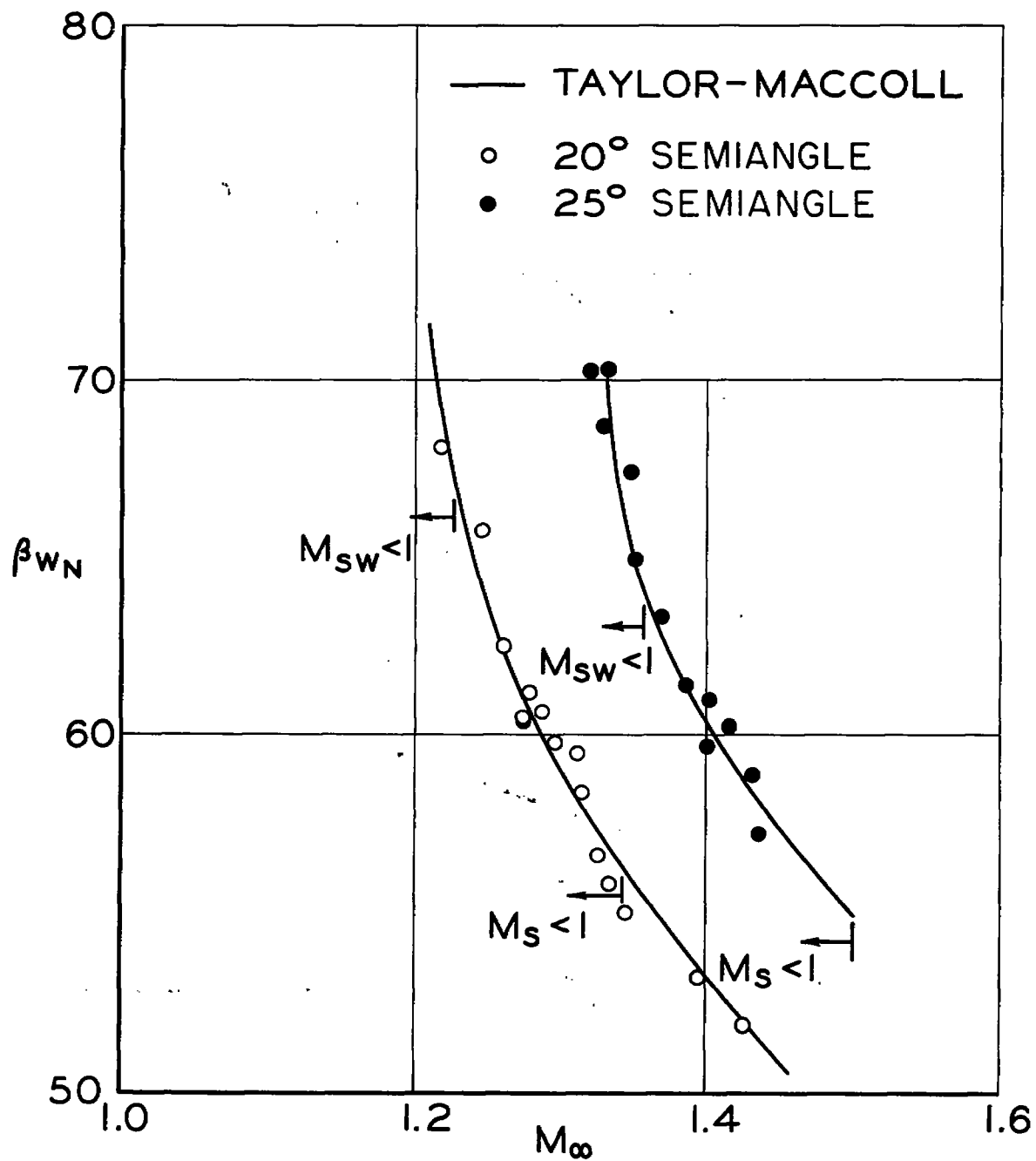
Figure 9.- Nose wave angle.
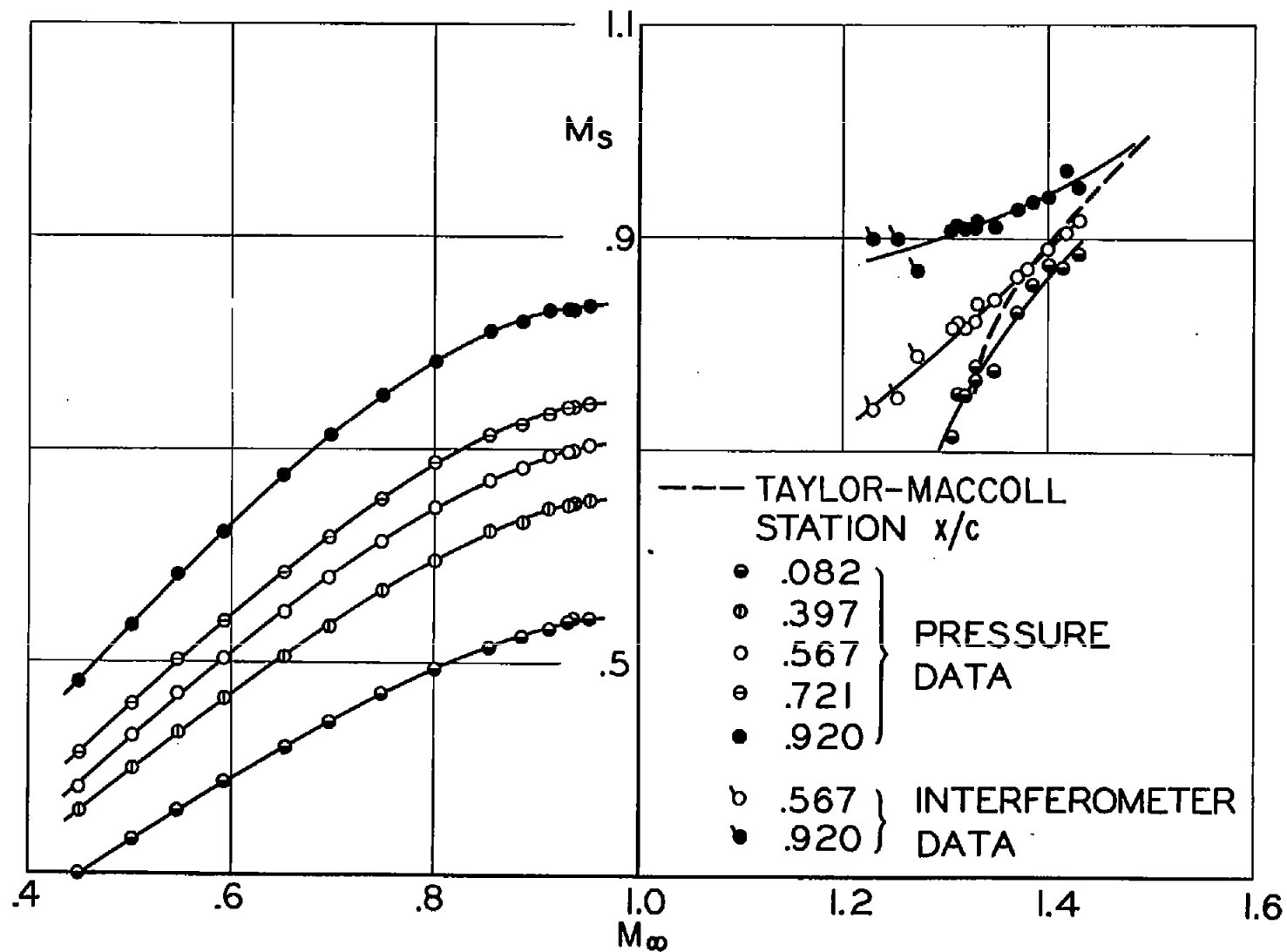
Figure 10.- Surface Mach number on 25° semiangle cone cylinder.
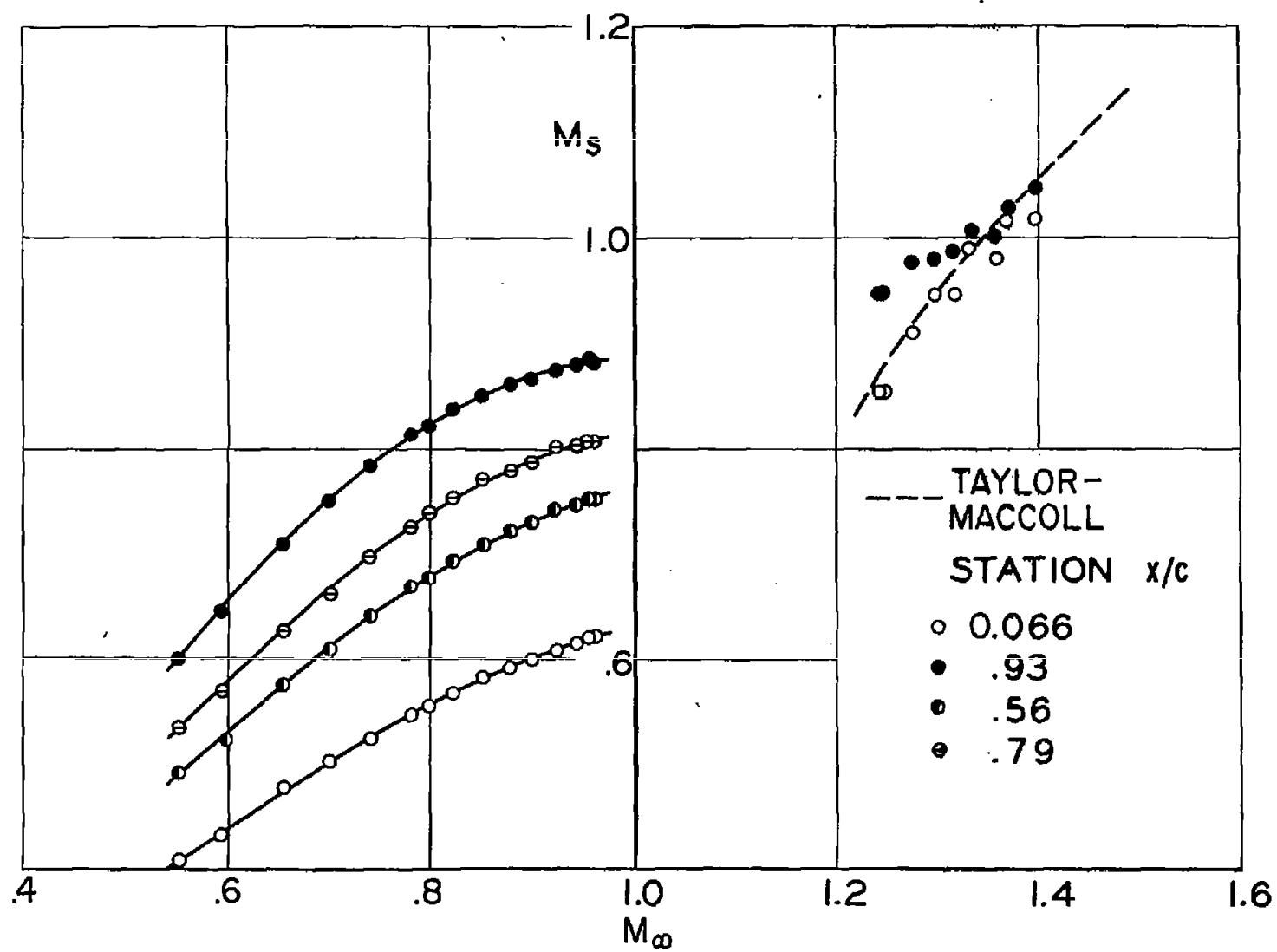
Figure 11.— Surface Mach number on 20° semiangle cone cylinder.
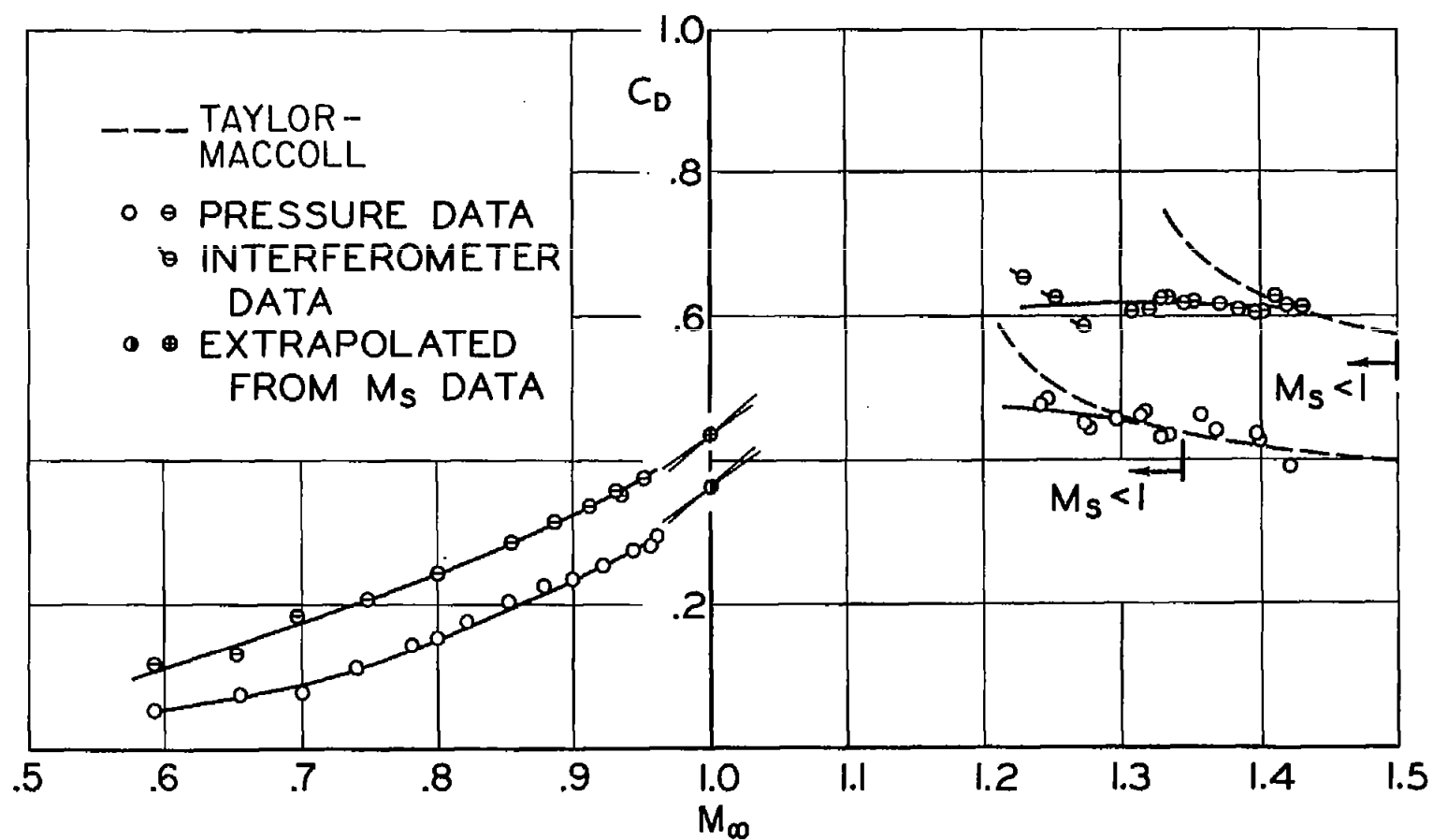
Figure 12.- Drag coefficients for cone cylinders.
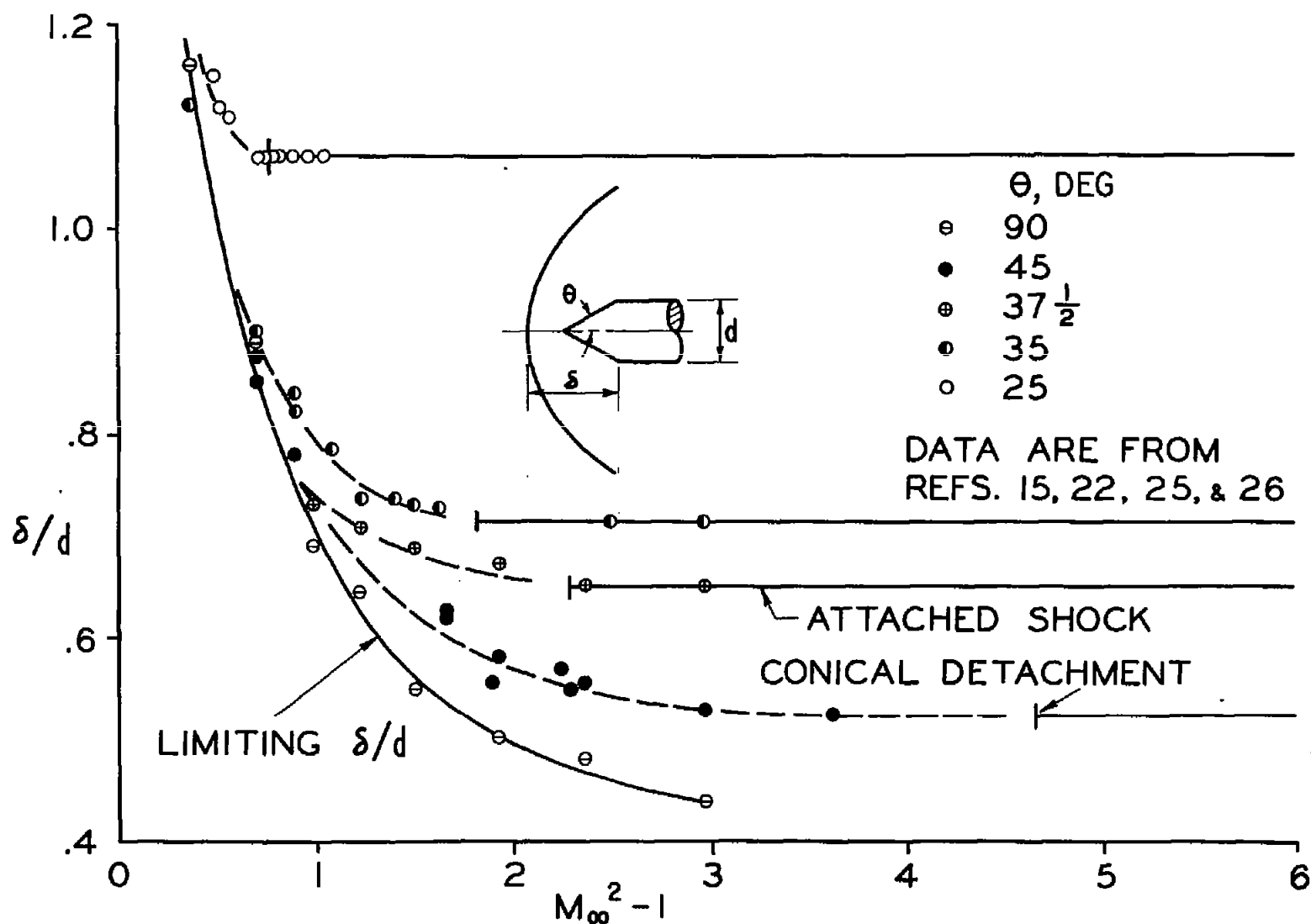
Figure 13.- Shock-wave detachment distance for finite cones. Data are from references 15, 22, 25, and 26.
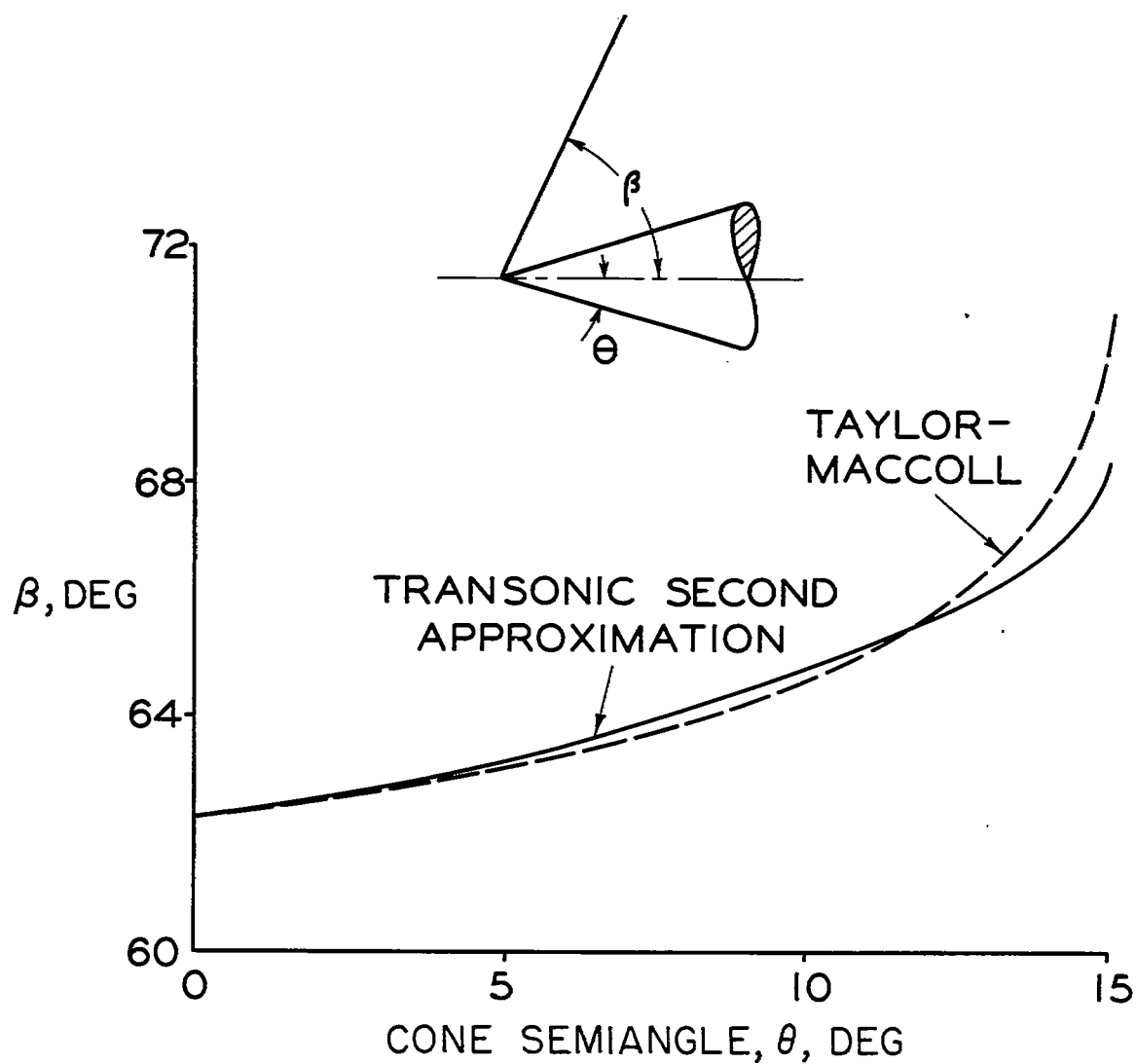
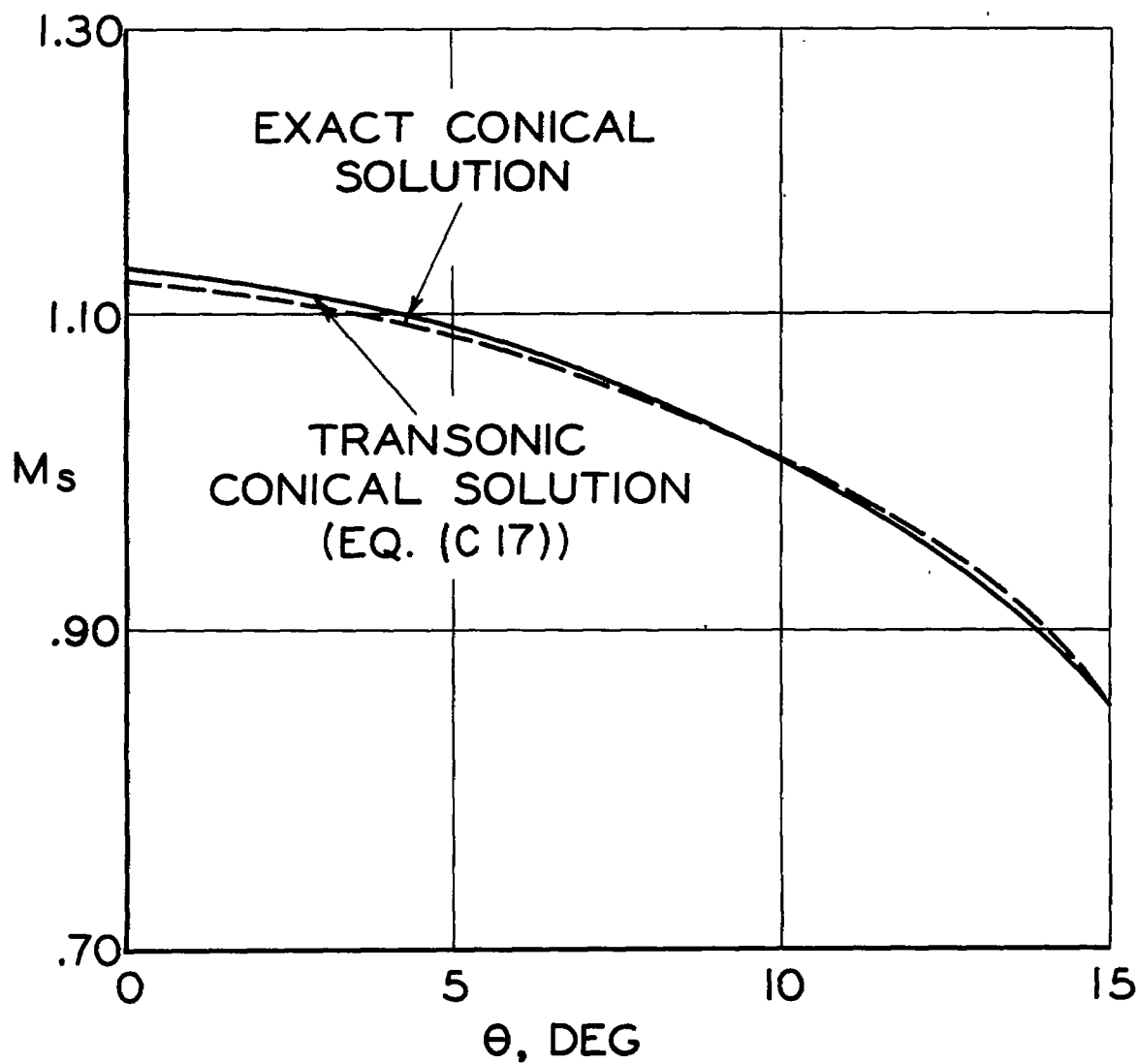Figure 14.- Shock-wave angle for semi-infinite cones. $u_\infty = 0.25$; $M_\infty = 1.12$.

Figure 15.- Transonic conical solution; surface Mach number versus cone semiangle. $u_\infty = 0.25$; $M_\infty = 1.12$. (M_∞ is defined as $M_\infty = \sqrt{1 + u_\infty}$.)
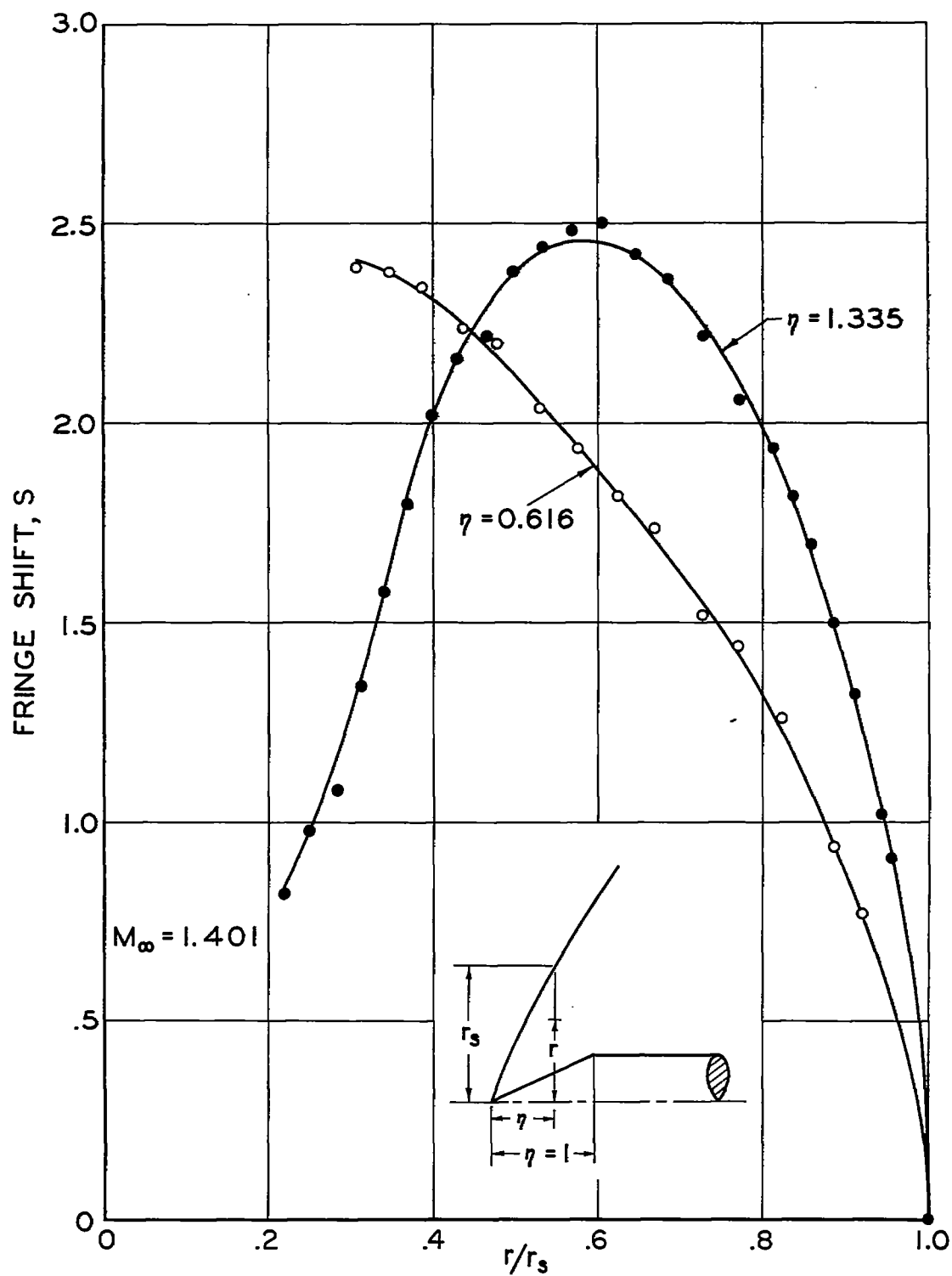
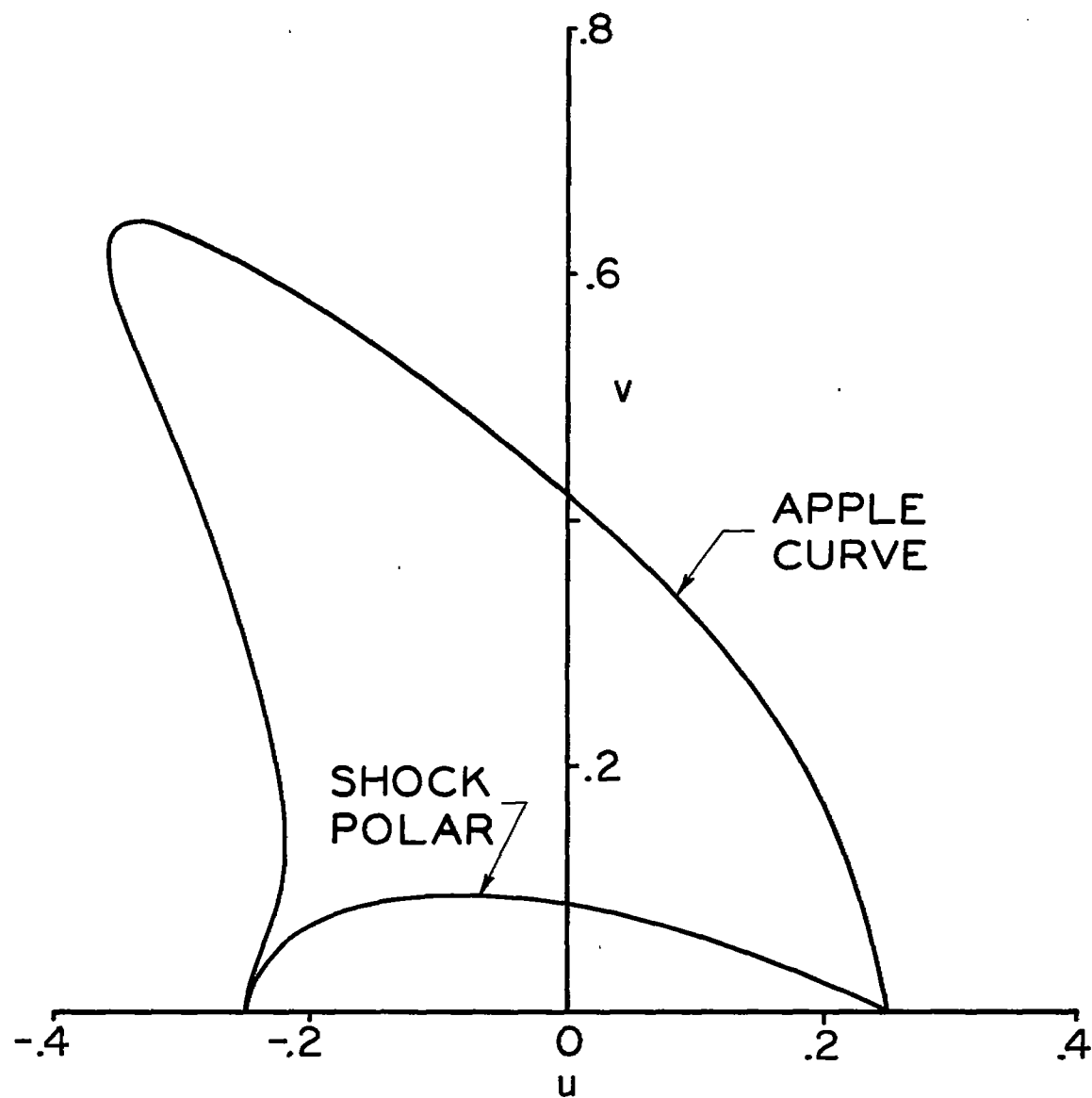Figure 16.- Interferogram fringe shifts for 25° semiangle cone cylinder.

Figure 17.- Transonic apple curve at $u_\infty = 0.25$ from second approximation.